Dannberg, J., Eilon, Z., Faul, U., Gassmoeller, R., Moulik, P., & Myhill, R. (2017). The importance of grain size to mantle dynamics and seismological observations. *Geochemistry, Geophysics, Geosystems*, *18*(8), 3034-3061. https://doi.org/10.1002/2017GC006944

The importance of grain size to mantle dynamics and seismological observations

J. Dannberg[1,2], Z. Eilon[3,4], U. Faul[5], R. Gassmöller[1,2], P. Moulik[6], R. Myhill[7]

[1]Department of Mathematics, Texas A&M University, College Station, TX 77843-3368, USA
[2]Department of Mathematics, Colorado State University, Fort Collins, CO 80523-1874, USA
[3]Department of Earth, Environmental, and Planetary Sciences, Brown University, Providence, RI 02912, USA
[4]Department of Earth Sciences, University of California Santa Barbara, Santa Barbara, CA 93106-9630, USA
[5]Earth, Atmospheric and Planetary Sciences, Massachusetts Institute of Technology, Cambridge, MA 02139, USA
[6]Department of Geology, University of Maryland, College Park, MD 20742, USA
[7]School of Earth Sciences, University of Bristol, Wills Memorial Building, Queen's Road, Bristol BS8 1RJ, UK

Key Points:

- We have implemented dynamically evolving grain size into whole mantle flow models, for which we compute seismological parameters
- Preferred models show lateral viscosity variations of up to six orders of magnitude in the mantle and positive strain rate feedbacks
- Seismic attenuation predictions help constrain lower mantle anelasticity. Grain size variation modulates simple thermal effects on velocity

Corresponding author: J. Dannberg, judannberg@gmail.com

Abstract

Grain size plays a key role in controlling the mechanical properties of the Earth's mantle, affecting both long-timescale flow patterns and anelasticity on the timescales of seismic wave propagation. However, dynamic models of Earth's convecting mantle usually implement flow laws with constant grain size, stress-independent viscosity, and a limited treatment of changes in mineral assemblage. We study grain size evolution, its interplay with stress and strain rate in the convecting mantle, and its influence on seismic velocities and attenuation. Our geodynamic models include the simultaneous and competing effects of dynamic recrystallization resulting from dislocation creep, grain growth in multiphase assemblages, and recrystallization at phase transitions. They show that grain size evolution drastically affects the dynamics of mantle convection and the rheology of the mantle, leading to lateral viscosity variations of six orders of magnitude due to grain size alone, and controlling the shape of upwellings and downwellings. Using laboratory-derived scaling relationships, we convert model output to seismologically-observable parameters (velocity, attenuation) facilitating comparison to Earth structure. Reproducing the fundamental features of the Earth's attenuation profile requires reduced activation volume and relaxed shear moduli in the lower mantle compared to the upper mantle, in agreement with geodynamic constraints. Faster lower mantle grain growth yields best fit to seismic observations, consistent with our re-examination of high pressure grain growth parameters. We also show that ignoring grain size in interpretations of seismic anomalies may underestimate the Earth's true temperature variations.

1 Introduction

The evolution and spatial distribution of grain size are some of the most important but weakly constrained characteristics controlling deformation in the Earth's mantle. Grain size may play a major role for the convective regime of terrestrial planets [*Rozel*, 2012] and the onset of convective instabilities [*Hall and Parmentier*, 2003], the thermal evolution of the Earth [*Solomatov*, 2001; *Rozel*, 2012], plume morphology [*Korenaga*, 2005], development of lattice preferred orientation and seismic anisotropy [*Podolefsky et al.*, 2004; *Becker et al.*, 2008; *Behn et al.*, 2009], the permeability structure and focusing of melt towards mid-ocean ridges [*Turner et al.*, 2015], as well as earthquake generation and shear-zone formation [*Montési and Hirth*, 2003; *Thielmann et al.*, 2015]. Moreover, grain size not only affects long timescale geodynamics, but also the propagation of seismic waves. The relationships between intrinsic variables (e.g. pressure, P; temperature, T; grain size, d) and seismically

observed parameters (seismic velocities, V; attenuation, Q^{-1}) are a topic of active research [*Faul and Jackson*, 2005; *Jackson and Faul*, 2010; *McCarthy et al.*, 2011; *Priestley and McKenzie*, 2013; *Takei et al.*, 2014; *Faul and Jackson*, 2015; *Yamauchi and Takei*, 2016]. Thermo-chemical interpretations of seismic anomalies are likely to be more accurate when the competing effects of grain size are taken into consideration.

Grain size influences mantle rheology and flow, but in turn, the deformation mechanisms in the Earth's mantle also affect grain size evolution. Some strain is accommodated by grain boundary diffusion in the diffusion creep regime. A rock with small grains will have a higher volumetric proportion of grain boundaries, and will therefore exhibit a lower effective viscosity at a given stress. As grain growth is faster at higher temperatures, it has been argued that the higher grain size within hot plumes could result in a higher viscosity than the rest of the mantle [*Solomatov*, 1996; *Karato*, 1997; *Solomatov et al.*, 2002; *Korenaga*, 2005]. For similar reasons, it has been suggested that cold slabs could be less viscous than warmer slabs in the mantle transition zone [*Karato et al.*, 2001]. Conflicting ideas surround possible behavior in the uppermost lower mantle; slabs have been suggested to be weak due to small grains [*Ito and Sato*, 1991] or interconnected ferropericlase [*Yamazaki et al.*, 2014], or strong through the formation of a perovskite-periclase symplectite texture [*Zhao et al.*, 2012].

Grain size evolution is also affected by deformation processes. The propagation of dislocations through grains causes dynamic recrystallization, which reduces grain sizes and hence promotes diffusion creep. This interplay between creep mechanisms and grain size reduction tends to cause strain localization [*Vauchez et al.*, 2012], which may affect many processes, including the formation of tectonic plates [*Bercovici and Ricard*, 2014] and the ascent velocities of mantle plumes. The heterogeneous and time-dependent distribution of stress and deformation in the mantle therefore leads to a strong spatial variability of the grain size reduction and thus causes strong lateral contrasts in grain size and viscosity.

Finally, the grain size is also influenced by phase transformations. While crossing polymorphic phase transitions such as olivine–wadsleyite and wadsleyite–ringwoodite is expected to have almost no influence on the grain size, when ringwoodite breaks down to bridgmanite and magnesiowüstite the grain size is likely to be reduced to approximately 1 μm [*Solomatov and Reese*, 2008]. This effect reduces variable grain sizes in chemically heterogeneous mantle material to a uniform grain size, which could negate grain size related

viscosity contrasts and may affect the efficiency of mantle mixing [*Solomatov and Reese*, 2008].

Seismological observations of travel times and quality factors give key insights into intrinsic elastic and anelastic structure of the present-day Earth [e.g. *Dziewonski and Anderson*, 1981]. Time-dependent grain-scale relaxation processes can act at seismic frequencies of seconds to minutes, such that the Earth acts as an anelastic medium [*Goetze*, 1977]. Like viscosity, these relaxation processes are related to the movement and propagation of defects and grain boundaries [e.g. *Karato and Spetzler*, 1990]. The resulting seismic attenuation and the associated velocity dispersion are measured at various frequencies (~1–3000s), potentially providing indirect constraints on the grain-size distribution in the mantle. Synthetic seismic data therefore allows us to interrogate model structure and provides a self-consistent approach to quantitatively compare model outputs with each other and (in aggregate, if not specific, terms) with the real Earth.

Despite its importance for mantle flow and seismic interpretation, the influence of grain size evolution on mantle dynamics, seismic velocities and attenuation is poorly understood. In particular, coupled grain size evolution and grain-size dependent rheology using Earth-like parameters for grain growth and grain size reduction have not yet been incorporated in global two- or three-dimensional mantle convection models. Although these effects have been considered in regional convection models [e.g. *Turner et al.*, 2015], studies of large-scale mantle flow have neglected or simplified grain size evolution [*Solomatov and Reese*, 2008; *Rozel*, 2012], and generally did not consider the dependence of grain size evolution parameters on the mineral phase [*Rozel*, 2012; *Solomatov and Reese*, 2008; *Hall and Parmentier*, 2003]. So far, the involved numerical challenges have prevented more realistic models – an obstacle we are now able to overcome by using modern numerical methods and by making use of the increased availability of computational resources.

We follow a two-step approach and focus on certain aspects of this multi-disciplinary problem. Firstly, we study how a dynamically evolving grain size influences lateral viscosity variations in the mantle and investigate potential implications for the mantle viscosity profile. We strive to understand how dynamics and mixing of upwelling plumes and subducted slabs are affected by these viscosity variations, and which of the current concepts and assumptions about mantle convection have to be reconsidered for a mantle with dynamically evolving grain size. We then link the outputs of our geodynamic models to experimentally-

constrained scaling relationships that allow us to predict seismologically-observable features, resolving trade-offs between temperature and grain size in controlling the (an)elastic behavior of rocks. By comparing model predictions to large-scale Earth velocity and attenuation structure, we can constrain thermodynamic parameters at conditions inaccessible in the laboratory, reciprocally constraining parameters used for the dynamical simulations.

2 Methods

We use existing experimental data for grain growth and rheological parameters for the main mantle mineral phases and apply them in geodynamic models of global mantle convection. Our models include the effects of grain growth and grain size reduction. Grain size reduction encompasses both dislocation creep and decomposition reactions, fully coupled with mantle convection with a composite diffusion/dislocation rheology that depends on the dynamically evolving grain size. We compare models with and without grain size evolution, and investigate the influence of varying some of the parameters that control grain growth. To compute seismic properties from the output of these models, we apply experimentally constrained anelastic scaling relationships modified (where appropriate) for consistency with the thermodynamic parameters used in the geodynamic models. These relationships quantify the roles of grain size, temperature, and pressure for determining seismic velocity and attenuation, allowing us to predict the whole mantle seismic structure for each model. We grid search through the parameter space of the poorly-constrained lower mantle relaxation strength and activation volume, comparing model results to Earth structure to place quantitative bounds on lower mantle anelastic behavior at conditions inaccessible to laboratory experiments. The following sections will discuss these methods in detail.

2.1 Rheology

The rheology implemented in this study includes diffusion and dislocation creep, which are governed by expressions of the form (see Text S1.1):

$$\eta = \frac{1}{2} A^{-\frac{1}{n}} d^{\frac{m}{n}} \dot{\varepsilon}_{\mathrm{II}}^{\frac{1-n}{n}} \exp\left(\frac{E^* + PV^*}{nRT}\right), \tag{1}$$

where d is the (variable) grain size, $\dot{\varepsilon}_{\mathrm{II}}$ is the square root of the second invariant of the strain rate tensor, A is a constant prefactor, E^* and V^* are the activation energy and volume, and P, R and T are the pressure, gas constant and temperature. The diffusion creep viscosity η_{diff} is typically strain rate independent ($n = 1$), and the dislocation creep viscosity η_{dis} is usually

grain size independent ($m = 0$), leading to the expressions used in our model:

$$\eta_{\text{diff}} = \frac{1}{2} A_{\text{diff}}^{-1} d^m \exp\left(\frac{E^*_{\text{diff}} + PV^*_{\text{diff}}}{RT}\right), \tag{2}$$

$$\eta_{\text{dis}} = \frac{1}{2} A_{\text{dis}}^{-\frac{1}{n}} \dot{\varepsilon}_{\text{dis,II}}^{\frac{1-n}{n}} \exp\left(\frac{E^*_{\text{dis}} + PV^*_{\text{dis}}}{nRT}\right), \tag{3}$$

and the effective viscosity

$$\eta_{\text{eff}} = \frac{\eta_{\text{diff}}\,\eta_{\text{dis}}}{\eta_{\text{diff}} + \eta_{\text{dis}}}. \tag{4}$$

All of the rheological parameters depend on the current mineral phase and are listed in Tables S1 and S2. The diffusion creep parameters of ringwoodite and bridgmanite, which we assume to be the rheologically dominant phase in the lower mantle, were computed from estimates of grain boundary diffusion following *Frost and Ashby* [1982] (see Text S1.2). We note that experimentally defined prefactors are sometimes based on different definitions of the strain rate (for example the norm or strain rate along the principal strain axis). In these cases, we have converted the prefactors (see Text S1.3). Also note that by setting $A_{\text{dis}} \ll A_{\text{diff}}$ for the bridgmanite & periclase phase, we assume that diffusion creep is always the dominating deformation mechanism in the lower mantle (see Text S1.4). After estimating all of the parameters, the power law prefactors were adjusted to match reasonable viscosity profiles for the Earth [e.g. *Mitrovica and Forte*, 2004; *Steinberger and Calderwood*, 2006] (see Text S1.5).

2.2 Grain size evolution

Grain growth in the present study is approximated using semi-empirical expressions of the form [e.g. *Burke*, 1949; *Austin and Evans*, 2007]:

$$\dot{d}_{\text{growth}} = p_g^{-1} d^{1-p_g} k_g \exp\left(-\frac{E_g + PV_g}{RT}\right) \tag{5}$$

where k_g is an experimentally determined prefactor, and E_g and V_g are the grain growth activation energy and volume. The term p_g is a grain growth exponent that is largely a function of the mechanism by which elements diffuse in the medium. Growth controlled by volume diffusion results in $p_g = 3$ [*Lifshitz and Slyozov*, 1961; *Wagner*, 1961], while if grain growth is controlled by grain boundary (surface) or dislocation (pipe) diffusion, $p_g = 4$ and $p_g = 5$ [*Ardell*, 1972]. Higher effective values have been reported, and are commonly attributed to elastic stress, impurities or the initial microstructure (grain size distribution or morphology; see *Solomatov et al.* [2002] for more details).

Grain size reduction is approximated by the paleowattmeter [*Austin and Evans*, 2007], where a certain fraction of the work done by dislocation creep goes into reducing the grain size (see Text S2):

$$\dot{d}_{\text{reduce}} = 4\,\dot{\varepsilon}_{\text{II}}\,\dot{\varepsilon}_{\text{dis,II}}\,\eta_{\text{eff}}\,\frac{\lambda d^2}{c\gamma}, \tag{6}$$

where c is a geometric constant, λ is the fraction of work that goes into changing the grain boundary area, and γ is the average specific grain boundary energy.

By equating the two sides of these expressions and using the equality of Equations (S25) and (S27) (see Text S2), an equilibrium grain size can be found for any given strain rate and temperature, where the competing effects of grain size reduction in the dislocation creep regime and grain growth in the diffusion creep regime are balanced:

$$d_{\text{eqm}} = \left(\frac{c\gamma k_g}{\lambda\sigma\dot{\varepsilon}_{\text{dis}} p_g}\exp\left(-\frac{E_g + PV_g}{RT}\right)\right)^{\frac{1}{1+p_g}} \tag{7}$$

Throughout the rest of the manuscript, we will refer to this paleowattmeter grain size as the equilibrium grain size. All grain size evolution parameters used in this study are listed in Table S1 and Table S2, they are discussed in more detail in Text S2.2. The upper mantle rheologies are also shown graphically Figure 1, along with the position of the equilibrium grain size. For low strain rates and small grain sizes, diffusion creep is the dominant deformation mechanism, and there is almost no dependence of viscosity on the strain rate. For high strain rates and large grains, dislocation creep is dominant, and the viscosity mainly depends on the strain rate. For intermediate values, both creep mechanisms are important. As grain growth is faster for smaller grain sizes, and grain size reduction is proportional to the dislocation strain rate, grains will evolve toward a single equilibrium size for any given strain rate (or stress). Notice that the equilibrium grain size line for each phase assemblage does not lie at the same position relative to the field boundary (where diffusion and dislocation creep strain-rate are equal contributors to the total strain rate). The position of the line is a function of the grain growth and creep law parameters.

We note that the sequence of mineral transformations in the Earth's mantle and therefore grain growth evolution is more complex than outlined in this study. Nevertheless, the current approach is reasonable given the paucity of experimental data.

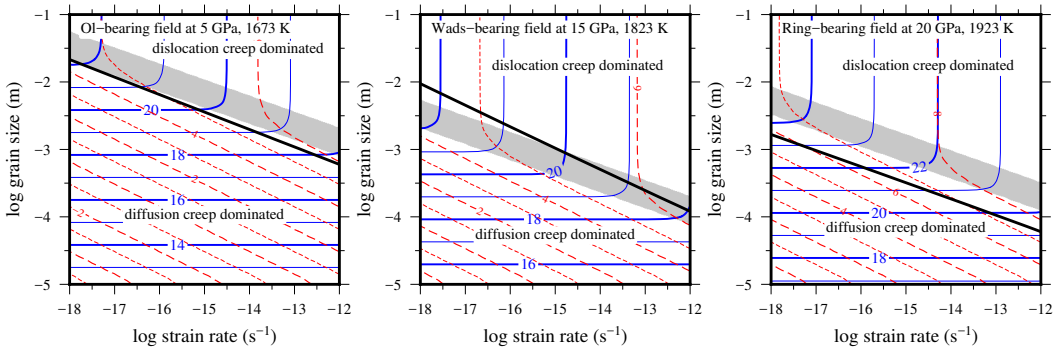

Figure 1. Viscosity and stress as a function of total strain rate and grain size for the three distinct upper mantle assemblage fields used in our simulations. Solid blue and red dashed contours mark lines of constant viscosity and stress respectively (labeled with the decadic logarithm of the value in Pa s or Pa). In diffusion-dominated creep, viscosity is grain size dependent and strain rate independent, such that viscosity contours are horizontal. The opposite is true of dislocation-dominated creep, where viscosity contours are vertical. The grey bands mark where diffusion and dislocation creep each contribute >10% of the total strain rate. The equilibrium grain size is shown as a black solid line. If this equilibrium grain size falls into the diffusion or dislocation creep regime is determined by a combination of the grain growth and rheologic parameters (see Section S5.1). In simulations with constant grain size, model viscosities (at constant temperature and pressure) would be uniquely constrained by the strain rate (or stress). By allowing grain size to vary, model viscosities can take a range of values. At fixed stress or strain rate, grains will tend to evolve towards the equilibrium grain size.

2.3 Geodynamic model

2.3.1 Equations

We use the mantle convection code ASPECT [*Kronbichler et al.*, 2012; *Bangerth et al.*, 2017] that models thermo-chemical convection in high Rayleigh number flow with adaptive mesh refinement. It solves the equations for the conservation of mass, momentum and energy, and an evolution equation for the grain size (see Text S2). Our models include adiabatic heating, shear heating, latent heat, radiogenic heat production and take into account mantle compressibility. Specifically, we consider the following set of equations for velocity $\mathbf{u}$, pressure p, temperature T and grain size d:

$$-\nabla \cdot (2\eta \dot{\varepsilon}_\kappa(\mathbf{u})) + \nabla p = \rho \mathbf{g}, \tag{8}$$

$$\nabla \cdot (\rho \mathbf{u}) = 0, \tag{9}$$

$$\rho C_p \left(\frac{\partial T}{\partial t} + \mathbf{u} \cdot \nabla T \right) - \nabla \cdot k \nabla T = 2\eta \dot{\varepsilon}_\kappa(\mathbf{u}) : \dot{\varepsilon}_\kappa(\mathbf{u}) + \alpha T \, (\mathbf{u} \cdot \nabla p) + Q \tag{10}$$

$$\left(\frac{\partial d}{\partial t} + \mathbf{u} \cdot \nabla d \right) = p_g^{-1} d^{1-p_g} k_g \exp\left(-\frac{E_g + PV_g}{RT} \right) - 4 \, \dot{\varepsilon}_{\mathrm{II}} \, \dot{\varepsilon}_{\mathrm{dis,II}} \, \eta_{\mathrm{eff}} \frac{\lambda d^2}{c\gamma}, \tag{11}$$

where $\dot{\varepsilon}_\kappa(\mathbf{u}) = \frac{1}{2}(\nabla \mathbf{u} + \nabla \mathbf{u}^T) - \frac{1}{3}(\nabla \cdot \mathbf{u})\mathbf{1}$ is the compressible strain rate. The material parameters density ρ, specific heat C_p and thermal expansivity α are computed as a function of pressure and temperature using the thermodynamic calculation package HeFESTo [*Stixrude and Lithgow-Bertelloni*, 2005, 2011] and assuming a pyrolitic composition [*Xu et al.*, 2008; *Workman and Hart*, 2005]. Latent heat effects are accounted for by modifying α and C_p to effective values incorporating the temperature and pressure entropy derivatives [*Nakagawa et al.*, 2009; *Gerya et al.*, 2004]. We use a radiogenic heat production of $Q = 6 \times 10^{-12}$ W/kg in agreement with other modeling studies and slightly above proposed bulk-silicate-earth compositions [*Nakagawa et al.*, 2009; *Jaupart et al.*, 2015]. The thermal conductivity is fixed to $k = 4$ W/mK, and the effective viscosity η is described in Section 2.1.

Upon crossing the ringwoodite ↔ bridgmanite + periclase phase transition the grain size is reset, following previous studies [*Solomatov and Reese*, 2008]. We choose a fixed reset value of 20 μm (post-reaction grain size in Table S1), which avoids convergence problems at very low model viscosities. In experiments, the transformation creates even smaller grain sizes [*Poirier et al.*, 1986; *Ito and Sato*, 1991], but growth from sub-micron sizes to 20 μm is predicted to occur within a few thousand years – approximately one time step in our

models. The exact choice of reset value therefore does not affect the model results on a large scale.

2.3.2 Numerical challenges

Modeling mantle convection with an evolving grain size and grain size dependent rheology is numerically challenging for several reasons. We address these challenges using modern numerical methods.

(1) The positive feedback between shear-induced grain size reduction and grain-size-controlled viscosity reduction leads to strain localization, high viscosity contrasts, and small-scale convection features. ASPECT's adaptive mesh refinement allows us to refine the mesh in these regions, requiring significantly fewer computational resources compared to an equally accurate model with uniform mesh. Parallelization of the code allows global models with a local resolution of approximately 6 km.

(2) The strong non-linear dependence of the viscosity on temperature, grain size, and stress/strain rate leads to steep local viscosity gradients as well as large global contrasts: In the olivine phase, a temperature change of 150 – 200 K, a grain size variation of a factor of 2.2 or a strain rate variation of a factor of 30 result in a viscosity contrast of one order of magnitude, respectively. This demands robust non-linear solvers. ASPECT uses fixed-point iterations to resolve non-linearities in the equations, alternating between solving the Stokes system (Equations (8) and (9)), and the advection systems (Equations (10) and (11)) until convergence is reached. It employs a generalized minimal residual method with a Wathen style block preconditioner for the Stokes part of the problem, allowing for high local and global viscosity contrasts [*Kronbichler et al.*, 2012]. For this study, we choose to limit the global viscosity variation to a range of [10^{18} Pa s, 10^{24} Pa s]; the primary reason being the increase in velocity due to decreased viscosity and the associated shorter time steps.

(3) Finally, the grain size – here modeled as a continuous field – varies by several orders of magnitude, including steep gradients at phase transitions, potentially leading to instabilities such as over- and undershooting. In addition, grain growth and reduction depend on the the grain size itself and occur on a much shorter time scales than the advection, if the grain size is not close to the equilibrium. Thus, grain size can vary by more than one order of magnitude within one advection time step. ASPECT's higher order time stepping scheme BDF2, higher order finite elements, and entropy viscosity stabilization technique [*Guer-*

mond et al., 2011] allow a stable grain size advection. The nonlinear dependence of grain size growth on grain size is addressed by separately solving the ordinary differential equation for the evolution term on the right hand side of Equation (11) in each time step.

Taken together, these numerical challenges increase the computational cost of models with fully coupled grain size evolution and grain size dependent rheology approximately seven times compared to a conventional mantle convection model (see Text S3).

2.3.3 Model setup

The model domain is a two-dimensional spherical shell, including the whole mantle in vertical direction. The initial mantle temperature is adiabatic, with a potential temperature of 1600 K, a cold top boundary layer representing lithosphere with an age of 100 Ma and a hot bottom boundary layer consistent with 300 Ma of thermal diffusion. The boundary temperatures and velocities are prescribed throughout the model evolution, using the present-day plate velocities [*Gurnis et al.*, 2012] to generate subduction zones, and a core-mantle boundary temperature of 3486 K (which is equivalent to a temperature change of 750 K across the bottom thermal boundary layer) to allow for the ascent of mantle plumes. We chose this comparatively low temperature in comparison to commonly used values [3300 – 4400 K, *Boehler*, 2000; *Hernlund et al.*, 2005; *Lay et al.*, 2008] to match the excess temperatures of mantle plumes at the surface to the observations [200 – 300 K, e.g. *Herzberg and Gazel*, 2009; *Schilling*, 1991]. In addition, this is based on the fact that our models neglect chemical heterogeneities, and that the presence of a dense chemical boundary layer at the core–mantle boundary is expected to reduce the temperature of rising plumes compared to the bottom thermal boundary layer [*Farnetani*, 1997; *Lin and van Keken*, 2006]. The initial grain size follows a radial profile with values matching the equilibrium grain size for a reference temperature and pressure and an expected value for the strain rate for each phase.

We performed five computations with varying complexity, and let the models evolve for 300 Ma. Due to the high computational cost discussed in Text S3, we did not search a wide parameter range, but instead varied a few important parameters in the lower mantle, where experimental data are least well constrained, and fit the viscosity profile to match reasonable viscosity profiles for the Earth [*Mitrovica and Forte*, 2004; *Steinberger and Calderwood*, 2006]:

1. The *reference* model uses the parameters from the literature, modified as described in Section 2.1 and 2.2 and shown in Table S1.
2. For a second model we reduced the activation volume of diffusion creep in the lower mantle, because a preliminary model analysis indicated that the original value was too large to fit seismic observations (see Section 3.4). This reduces the vertical viscosity change within the lower mantle, but causes a higher viscosity contrast at the upper–lower mantle boundary (Model *LM-V_{diff}1.5e-6*). The pressure control on the activation volume originates from the understanding that the volume of lattice defects accommodating creep will decrease as pressure increases. Elastic strain laws can be used to estimate this volume dependence [e.g. *Poirier and Liebermann*, 1984]. We adopt a piecewise constant activation volume for simplicity.
3. Moreover, we derived a second set of parameters for grain growth in the lower mantle, using a grain growth exponent of $p_g = 5$, corresponding to dislocation-dominated diffusion, instead of the value directly derived from the experimental data (~11, see Text S2.3). This leads to faster grain growth and larger grains in the lower mantle (Model *faster-LM-grain-growth*). The model also uses the reduced diffusion creep activation volume.
4. For comparison, we also ran a model with a constant grain size for each phase, but a similar viscosity profile as in the *reference* model and diffusion–dislocation creep rheology (Model *constantGS*, see Supplementary Movie S2).
5. Finally, we included a model with only diffusion creep in the formulation of *Steinberger and Calderwood* [2006] to show how our results compare to commonly used viscosity formulations (see Supplementary Movie S1).

Average viscosity and grain size profiles for all models are shown in Figure S1 and S2, respectively, and the changed parameters are summarized in Table S2.

2.3.4 Translating physical properties to seismic structure: Modeling parameterizations

We use laboratory constrained relationships to predict seismically observable parameters from the output of the geodynamic models. The elastic and attenuating properties of a medium that influence the propagation of seismic waves (e.g. shear velocity, V_S; attenuation, Q_μ) are strong functions of its thermodynamic state. Scaling relationships between the

thermodynamical (e.g. pressure, P; temperature, T; grain size, d, composition, X) and seismological variables are typically derived based on empirical experimental data [e.g. *Jackson and Faul*, 2010; *Faul and Jackson*, 2015] and relaxation theory [e.g. *Minster and Anderson*, 1981; *Anderson and Minster*, 1981]. In particular, grain size is shown to have a strong effect on seismic variables: smaller grains decrease seismic velocities and increase seismic attenuation (Figure S3). Geodynamic model outputs are well suited for translation to seismological parameters because the thermodynamic variables at every point are known.

For a viscoelastic solid, the response to an imposed stress is frequency (ω) dependent and includes elastic, anelastic, and viscous terms. This response can be modelled with a Burgers model of the complex compliance, $J^*(\omega) = J_1(\omega) + iJ_2(\omega)$, where J_1 and J_2 are the storage and loss compliances, respectively. The compliance terms are functions of the Maxwell time (τ_M) and Δ, the relaxation strength or the fractional weakening of the relaxed response compared to the anharmonic response ($\Delta = (J_R - J_U)/J_U$). Shear velocity and Q_μ are calculated as $V_S = \sqrt{\rho^{-1}\left(J_1^2 + J_2^2\right)^{-1/2}}$ and $Q_\mu^{-1} = J_2/J_1$. Grain size enters these expressions through its exponential control on the Maxwell time and integration limits of the functional form

$$\tau_i \propto d^m f(T, P, \omega). \tag{12}$$

The complete set of equations describing the relationship is given in Text S4 while the values employed in our analysis are outlined in Table S3.

In the laboratory, (an)elastic behavior of rocks is investigated through creep tests and forced oscillation experiments [*e.g.*, *Cooper*, 2002; *Faul and Jackson*, 2005; *Sundberg and Cooper*, 2010; *Jackson and Faul*, 2010; *McCarthy et al.*, 2011; *Takei et al.*, 2014; *Yamauchi and Takei*, 2016]. Laboratory studies involve markedly smaller grain size and pressure than that of the Earth's mantle and current limitations preclude measurements relevant to the lower mantle. However, these experiments are used to determine the parameters that govern anelastic scaling relationships (Eq. S32–S35) that may be extrapolated to mantle conditions, allowing us to predict lower mantle seismic properties. We assume that the functional form of these relationships persists into the lower mantle [*e.g.*, *Abers et al.*, 2014; *Olugboji et al.*, 2013]. This is supported by experiments showing that a broad range of materials, including ceramics [*e.g.*, *Barnhoorn et al.*, 2016], silicates [*Jackson et al.*, 1992; *Gribb and Cooper*, 1998; *Jackson and Faul*, 2010], inorganic compounds [*McCarthy et al.*, 2011; *Takei et al.*, 2014; *Yamauchi and Takei*, 2016] and perovskite analogues [*Webb et al.*, 1999] display an

absorption band or "High Temperature Background" (HTB) behaviour (see also *Faul and Jackson* [2015]). These experiments indicate that the exponent α in frequency dependence of attenuation, described using the power law $Q_\mu \propto \omega^\alpha$, usually falls between 0.2–0.4 within the absorption band across the broad range of materials. In the absence of other constraints, we utilize the extended Burgers model of *Jackson and Faul* [2010]; *Faul and Jackson* [2015], modifying the activation energy and volume in the upper mantle for consistency with geodynamic models. We calculate the anelastic shear modulus and shear attenuation as a function of thermodynamic condition, grain size and frequency (Figure S3).

Since the parameters for the anelastic portion of the extended Burgers model of olivine (Eq. S32–S35) are best constrained among silicates, they are adopted here for the olivine polymorphs and bridgemanite. Seismic frequencies are well within the absorption band so that the viscous portion of the Burgers model (last term in Eq. S33) does not enter the calculations. While this approach neglects potentially diverging parameters for different materials, lack of detailed experimental constraints and the fact that seismically observed attenuation values are well fit by this model (see Section 3.4) support this approach. For consistency with the geodynamic simulations, we use values for the activation volume and energy that are the same as for diffusion creep throughout the upper mantle (Table S1). Within this general framework, we use the activation energy for the *reference* model in the lower mantle and explore ranges for parameters that are experimentally poorly determined. While the absorption band is comparatively well constrained, the broad peak or plateau at the transition from elastic to anelastic behaviour awaits robust experimental confirmation. We treat the presence of this peak as an open question, testing anelastic models with and without this feature (Section 3.4). The anelastic activation volume (V^*) for the lower mantle is also not directly constrained by experiments, and is poorly constrained by geodynamic models. Our approach is to test ranges for V^* and as the relaxation strength, Δ_B, searching for values that yield seismic models that are compatible with observations. We use the HeFESTo package [*Stixrude and Lithgow-Bertelloni*, 2005, 2011] to compute anharmonic elastic moduli (G_U) as a function of pressure and temperature, assuming a pyrolite composition [*Xu et al.*, 2008; *Workman and Hart*, 2005].

The observational constraints on elastic moduli and attenuation in the Earth come from the analysis of seismic waves at various frequencies. Seismological models of shear attenuation (Q_μ) often employ quality factors of surface wave and normal modes that afford sensitivity to the transition zone and mid-mantle [*e.g. Dziewonski and Anderson*, 1981; *Okal and Jo*,

1990; *Widmer et al.*, 1991; *Durek and Ekström*, 1996]. The common features in these studies include low Q_μ values in the uppermost mantle (~80–200 km), intermediate Q_μ values in the transition zone (200–650 km) and highest Q_μ values in the lower mantle. While several discrepancies persist in attenuation tomography [*Romanowicz and Mitchell*, 2015], all models show a somewhat abrupt jump to high Q_μ in the lower mantle that is significant beyond the 2-σ uncertainties on either side of the 650 km discontinuity as reported by *Resovsky et al.* [2005]. *Moulik* [2016] evaluated the robustness of this feature by modulating the jump in Q_μ through regularization and found that it is required to fit recent normal-mode observations. Other studies that employ teleseismic body waves at shorter periods (~2–20s) with sensitivity in the mid to lowermost mantle show Q_μ report slightly higher (but not infinite) Q_μ in this region [e.g. *Lawrence and Wysession*, 2006; *Hwang and Ritsema*, 2011; *Durand et al.*, 2013]. We compare predicted attenuation profiles to the model QL6 [*Durek and Ekström*, 1996] for simplicity and to manage the computational cost in our fitting procedure (Section 3.4).

3 Results

Before investigating the dynamics of convection models with fully coupled grain size evolution, we will discuss the resulting grain size distribution in our models and its effects on the viscosity profiles and lateral viscosity variations. This first step will help us to better understand in which ways grain size influences the rheology, and where in the mantle these effects are important. We will then discuss the effects of a variable grain size on mantle plumes and subducted slabs, and compare the seismic observables inferred from the geodynamic models to velocity and attenuation profiles of the Earth.

3.1 Grain size

Grain sizes in the deep Earth are poorly known, therefore we are unable to provide a detailed comparison between our results and observations. In the shallow mantle, olivine grain sizes are typically on the order of millimeters to centimeters, as indicated by grain sizes in ophiolitic and abyssal peridotites [see *Hirth and Kohlstedt*, 2003, and references therein]. Smaller olivine grains are often the result of low temperature mylonitization [grain size reduction to <10 microns; e.g. *Jaroslow et al.*, 1996], while fluids can promote the growth of much larger crystals [growth to >10 cm; e.g. *Kurat et al.*, 1982]. *Ave Lallemant et al.* [1980] noted that xenoliths from the Southern Africa and the Basin and Range exhibited a correla-

tion between grain size and apparent depth of equilibration. For samples which they inferred to be close to the base of the lithosphere (240 km and 80 km depth respectively), grain sizes reached 6–8 mm and 7–14 mm. The olivine grain sizes in our models (Figures 3a,b and S2) are on the order of 1–7 mm, which are somewhat smaller than those reported by *Ave Lallemant et al.* [1980]. The somewhat higher grain sizes in the xenolith samples may reflect a need for minor adjustments in our grain growth and rheological laws (see also Text S5.1). Alternatively, they may indicate the importance of metasomatic fluids and melts on enhancing grain size.

At greater depths, our reference model parameters result in grain sizes that decrease to 100s of microns in the mantle transition zone, and then 10s of microns in the lower mantle (Figure 3a). As detailed in the introduction, the grain growth laws in the lower mantle are poorly understood. Adjusting the grain growth law derived from the experimental value (where $p_g \sim 11$) to one where the grain growth exponent is more physically reasonable ($p_g = 5$), results in lower mantle grain sizes of 100s of microns, just slightly smaller than in the mantle transition zone (Figures S2, 4 and 5).

Generally, in ~70% of the upper mantle and transition zone, grain sizes in our models do not deviate from the equilibrium grain size by more than a factor of 3 (see Figures **??** and S4 and Text **??**). The exceptions are subducting slabs, regions of small-scale convection, around phase transitions and phases with slow grain growth. This implies that for applications not concerned with the dynamics of these features, approximating the grain size in the upper mantle by its equilibrium value would be reasonable. Regions where substantial deviations from the equilibrium grain size occur are discussed in more detail in Sections 3.3.1 and 3.3.2 below.

3.2 Lateral viscosity variations and global effects

To illustrate the effect of a variable grain size, we compare the viscosity profiles in models with different mantle rheologies. Most geodynamic models consider the effects of pressure (controlling the viscosity profile) and temperature (controlling lateral viscosity variations) on viscosity. Incorporating diffusion and dislocation creep leads to additional viscosity variations determined by the strain rate, weakening the material in regions of strong deformation. This mechanism is especially important in the asthenosphere: Due to the relative motion of plates and the underlying mantle, high stresses can be present at the base of

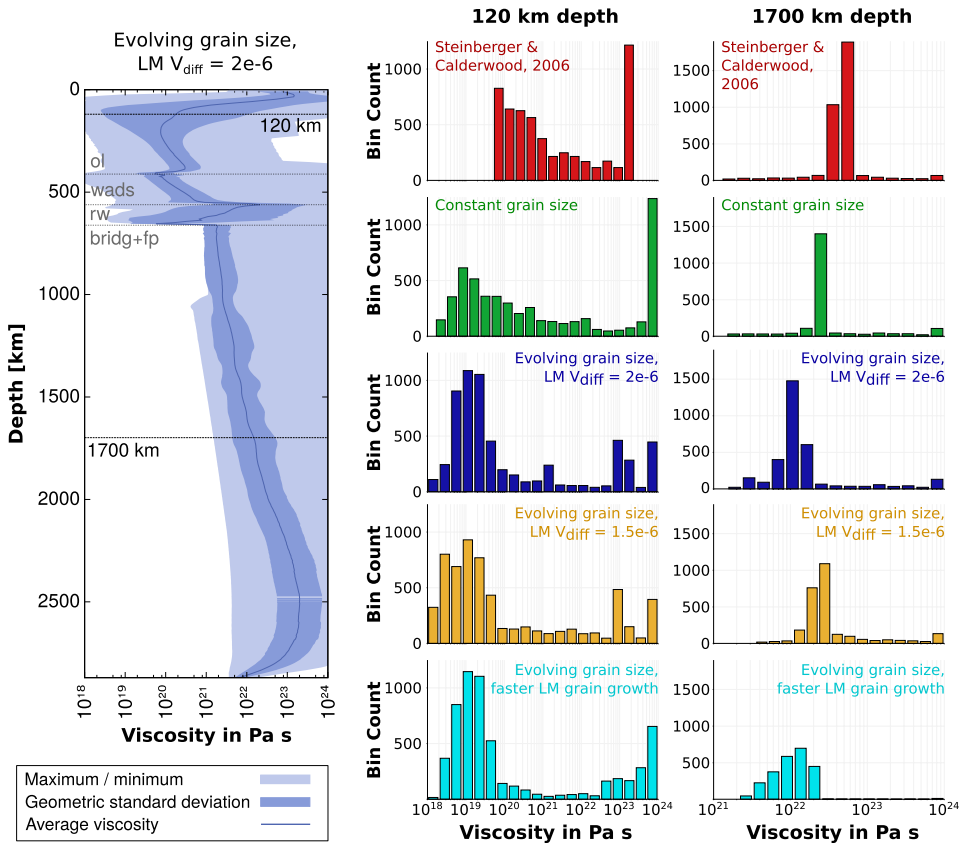

Figure 2. (Left) Radial average, minimum and maximum viscosity in the *reference* model at the end of the model evolution as a function of depth. Dashed gray lines mark phase transitions as given in Table S1. Variations above 650 km depth are mostly due to grain size and viscosity changes across phase transitions, the viscosity in the lower mantle reflects temperature and pressure changes with depth. (Right) Histograms of the viscosity distribution in a depth of 120 km (middle column) and 1700 km (right column) in models with and without grain size evolution, as detailed in Section 2.3.3 and Table S2. Viscosity variations are strongest below the base of the lithosphere and in models including grain size evolution.

the lithosphere, leading to a low viscosity and strong deformation in a thin layer. These effects are shown in Figure 2 (middle) and S1b, where the viscosity profile reaches much lower values in a depth of ~200 km compared to Figure S1a, which shows the viscosity profile of a model with only diffusion creep.

Considering the effect of grain size evolution on mantle rheology further increases the potential for lateral viscosity variations: In the upper mantle, grain size varies by almost two orders of magnitude at a given depth (Figure 3b), which results in viscosity variations of six orders of magnitude due to grain size alone (Figure 3c). In magnitude, these effects are comparable to the temperature-dependence of viscosity (cf. Text S5.2 and Figure S5). The influence of grain size is strongest in the upper mantle, because strong deformation can occur and both grain growth and grain size reduction are fast (Figure 3d). As there is a feedback between grain size and viscosity reduction, leading to larger deformation, the low-viscosity layer at the base of the lithosphere is even more pronounced (Figure 2) and shallower (~100 km depth, Figure S1c-e) than in models without grain size evolution. Grain size variations then generally decrease towards the lower mantle, where grain growth is slow, grain size reduction is negligible and the grain size is reset due to decomposition once material crosses the ringwoodite–bridgmanite phase transition.

As grain sizes in the upper mantle do not deviate much from their equilibrium value, the dominant deformation mechanism in each phase is mainly controlled by the the employed rheologic and grain growth parameters (cf. Figures 1, **??**, S4 and Text S5.1) rather than the model dynamics/strain rates. This is in contrast to models with a constant grain size, and should be taken into account for predictions of seismic anisotropy.

An exception is the layer of ringwoodite-bearing material immediately above the lower mantle, where grain sizes are strongly dependent on the P-T history of the material. This dependence is the result of slow grain growth relative to the time required to advect material through the layer, and leads to remarkably strong viscosity variations (Figure 3d). Upwelling material from the lower mantle with small grain sizes results in low viscosities regardless of temperature, and downwelling material with large grain size leads to higher viscosities (Supplementary Movie S3). This effect is also reflected in the negative slope of the viscosity profile and in the large standard deviation of both grain size and viscosity in the 520 – 650 km depth range (Figure 3b,c).

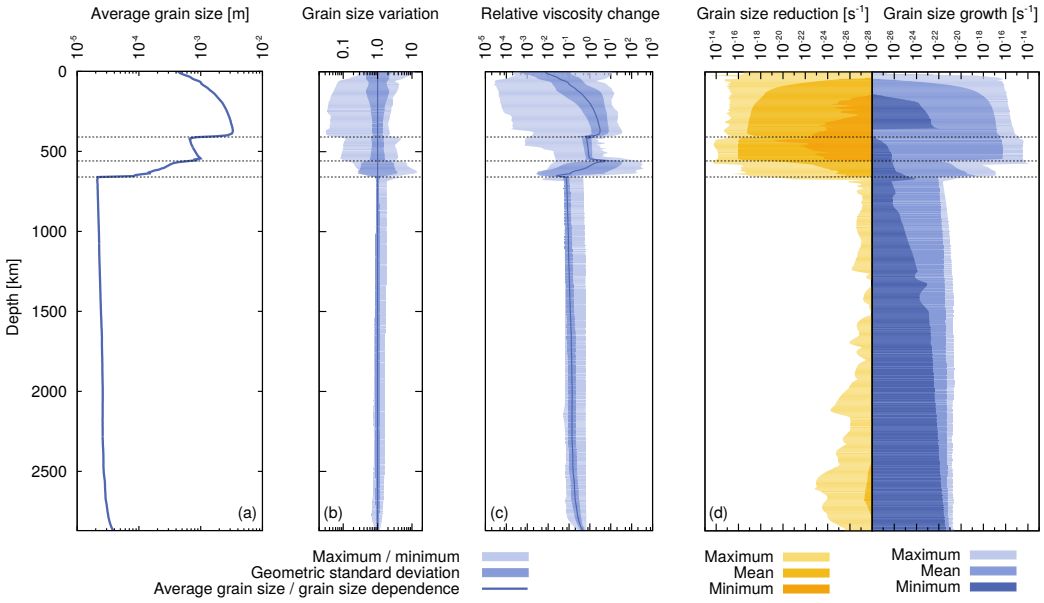

Figure 3. Lateral variations of grain size, viscosity and grain size growth/reduction in the *reference* model in dependence of depth. (a) Average grain size profile. (b) Relative lateral variations in grain size compared to the average for each depth. (c) Geometric mean and lateral variation of the viscosity due to grain size alone, illustrating the viscosity variations that are neglected when assuming a constant grain size in the rheology. Variations reach up to 6 orders of magnitude in the upper mantle (and 2 orders of magnitude in the geometric standard deviation). The relative viscosity change is computed by comparing the viscosity at any given point in the model to the viscosity at a reference grain size for that depth, all other variables being kept the same. Reference grain sizes are the same as in the *constantGS* model (see Figure S2a). (d) Minimum, maximum and geometric mean of grain growth and grain size reduction rate, showing which mechanism dominates for each given depth. The balance between both mechanisms in the upper mantle suggests that grains are generally close to the equilibrium grain size. Grain size reduction dominates the wadsleyite phase, whereas grain growth is dominant in the ringwoodite phase, but both processes are slower. Small ringwoodite grain sizes (despite grain growth being dominant) are mainly caused by upwelling of low-grain-size material from the lower mantle. Lower mantle grain growth occurs even more slowly, but is the only relevant process due to the absence of dislocation creep, indicating grain sizes far from their equilibrium value.

However, there are not only large differences between the models with and without grain size evolution, but also between the ones including grain size evolution, but employing different viscosity profiles (Model *LM-V_{diff}1.5e-6*) or grain size growth parameters (Model *faster-LM-grain-growth*) in the lower mantle. As the viscosity contrast between upper and lower mantle controls the dynamics of material passing through this transition, it plays an important role for the characteristics of mantle convection. A smaller activation volume does not crucially influence lateral viscosity variations (Figure 2 middle and right), but leads to a smaller viscosity gradient in the lower mantle and hence to a higher viscosity contrast at 650 km depth, if lowermost mantle viscosities are assumed to be on the order of $\sim 10^{23}$ Pa s (Figure S1c,d). Convection in the upper and lower mantle essentially become decoupled, and only plumes and slabs penetrate the transition (Supplementary Movie S4). This allows for a net rotation of the lower mantle, as velocities at the top are fixed to today's plate motions. Nevertheless, relative velocities between upper and lower mantle are small and lead to a total rotation of less than 45° over a timespan of 250 Ma, far below possible velocities of true polar wander on Earth [*Tsai and Stevenson*, 2007; *Steinberger and Torsvik*, 2008]. Due to the overall higher viscosity in this model, fewer plumes develop and they ascend more slowly (see Section 3.3.1), and slabs are slowed down and deformed strongly when they reach the lower mantle (see Section 3.3.2).

In contrast, a faster grain growth in the lower mantle changes both the viscosity profile and lateral variations drastically. In models with slow grain growth, grain size in the lower mantle is almost uniform and remains at the post-reaction grain size, except in hot plumes or strongly deformed slabs. Conversely, accelerated grain growth results in viscosities that are dependent on the residence time of material in the lower mantle. Downwelling material (such as around slabs) enters the lower mantle with a small grain size – resulting from decomposition – and low viscosities (assuming temperatures equal to the average mantle temperature). Over time, the grains grow and the viscosity increases (Supplementary Movie S5). This leads to strong lateral viscosity variations outside plumes and slabs (Figure 2, bottom row, and S1e), in the form of patches of "old" and "young" material adjacent to each other. In particular, if plumes and slabs are excluded, the geometric standard deviation of viscosity is much larger in the model with fast grain growth compared to the other models (for example, in 1700 km depth, it is 3 times larger than in the reference model). This means that the viscosity around subducted slabs can be one order of magnitude lower—and the viscosity of material accumulating at the base of the mantle can be one order of magnitude higher—than

the ambient mantle viscosity of material with the same temperature (which corresponds to the value expected for models without grain size evolution).

All of these scenarios seem plausible for the Earth's mantle and potentially have significant implications for mantle dynamics; hence, more accurate experimental or observational data are needed to constrain the viscosity parameter range.

3.3 Regional effects

In addition to its influence on the large-scale patterns of mantle convection, grain size evolution also has a strong effect on a smaller scale, and it affects the shape and dynamics of individual upwellings and downwellings in the mantle.

3.3.1 Mantle plumes

Viscosity is one of the key properties that controls the dynamics of ascending mantle plumes. In general high plume temperatures cause a decrease in viscosity and allow plumes to rise faster, however dynamic grain size evolution in plumes reveals two additional competing processes: High plume temperatures greatly accelerate grain growth, while high shear stresses caused by the relative movement between plume and surrounding mantle reduce the grain size. In the center of the plume, where temperatures are highest and stresses are lower, grains grow faster and become larger than in the surrounding mantle, in particular in the plume head. Most of the deformation, however, occurs at the edges of plumes, reducing the grain size compared to the adjacent mantle and decreasing the viscosity, which leads to strain localization. This results in a grain size variation of potentially more than one order of magnitude across the plume (Figure 4e,g,i, Figure S6). Consequently, the viscosity in the center of the plume is higher than at its edges and can reach the same values as in the surrounding mantle (Figure 4d,f,h). This is in contrast to plume models with classical viscosity formulations, where the viscosity is lowest in the hottest region in the plume center (Figure 4a,b). The localization of deformation also involves a strain rate variation of more than one order of magnitude across the plume, with the highest strain rates at its margins. Hence, the velocity profile across the plume tail is not a parabola or Gaussian as observed in models with constant grain size, but has steep gradients at the edges of the plumes and a nearly constant velocity in the plume center.

Compared to models with constant grain size (and in particular in comparison to models with only diffusion creep), upper mantle viscosities around plumes are lower in models with evolving grain size. Because of that, plumes in these models rise faster and flow between upper and lower mantle is more decoupled, which generally causes a stronger plume tilt (see Figure 4). When the rising plume spreads below the base of the lithosphere, high stresses arise between the plume and the overlying plate, reducing the grain size and consequently the viscosity. This process leads to higher strain rates and a faster lateral spreading of the plume. Hence, much stronger small-scale convection develops in the upper mantle, involving parts of sheared, delaminated lithospheric material (Figure 4d,f,h). This is in contrast to the more uniform flow field in models without grain size evolution (Figure 4a,b). However, the high plume spreading velocities in our models are consistent with the fast propagation and upwelling rates of plume head material required to explain the observations of V-shaped ridges in Iceland [*Ito*, 2001; *Jones et al.*, 2014; *Martinez and Hey*, 2017]. Different parameters for the lower mantle grain growth or diffusion creep activation volume do not change these general relations, and only influence the shape and timing of individual plumes. In contrast to the material ascending in the plume tail, plume material spreading below the lithosphere does not show such a strong shear localization at its edges (there is no "plug" flow, see Figure S7). Strong deformation at the base of the lithosphere reduces grain sizes by a factor of 3 compared to grain sizes in the spreading plume material, which leads to strong shear localization at the upper edge of the plume. However, due to the induced small-scale convection, velocity gradients in the bottom part of the plume are not as steep, and strain rates are similar to the ones in models with constant grain size.

3.3.2 Subducted Slabs

Not only the ascent of mantle plumes, but also the dynamics of slabs is changed by a grain-size dependent rheology. In models without grain size evolution, the shape of slabs is mainly controlled by the slab viscosity and the viscosity change across the 650 km discontinuity. Employing a viscosity formulation commonly used for mantle convection [*Steinberger and Calderwood*, 2006] leads to internal deformation and thickening of slabs when they reach the lower mantle, where they are slowed down by the higher ambient mantle viscosity (Figure 5a). Considering diffusion and dislocation creep increases the viscosity contrast between the inside and the edges of slabs, where the high strain rates weaken the material. Hence, slabs wriggle above the 650 km discontinuity, deforming less internally, and instead

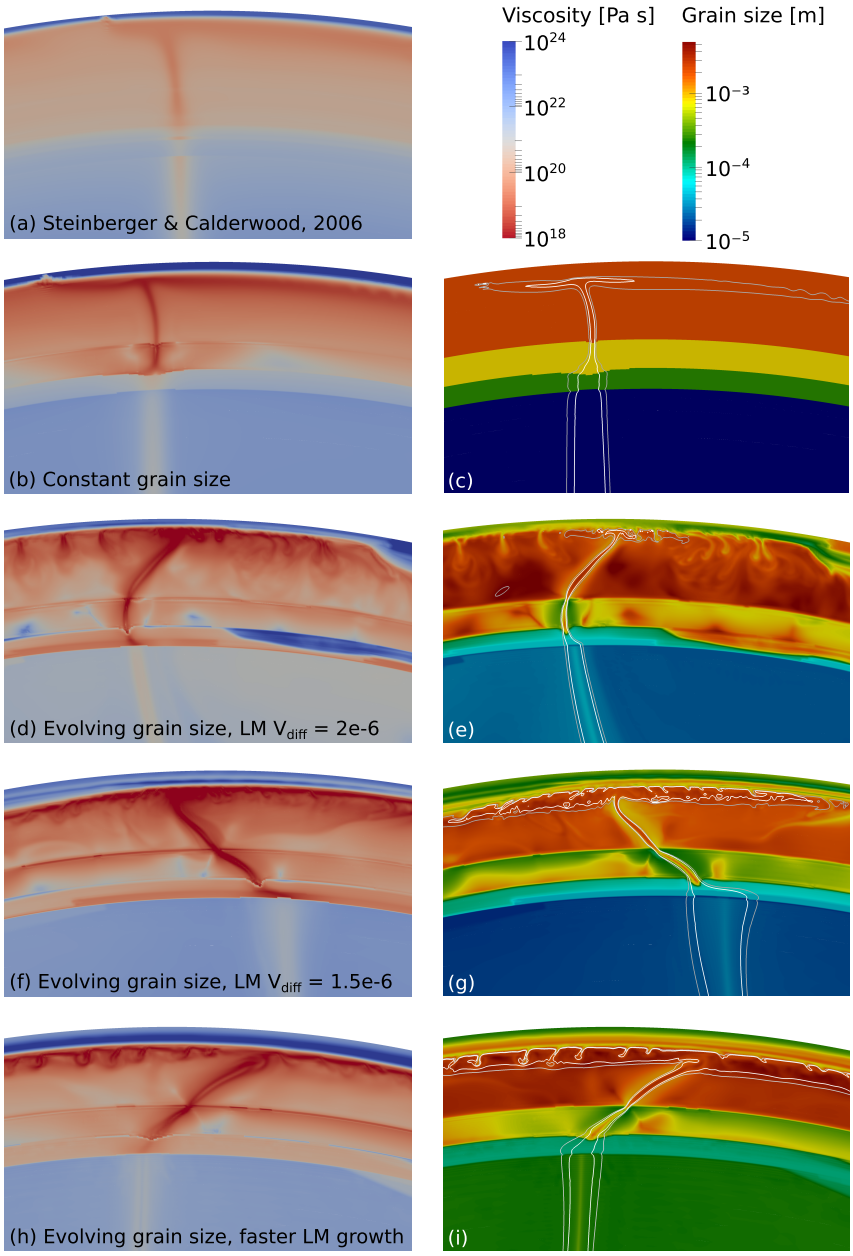

Figure 4. Shape and dynamics of mantle plumes in dependence of grain size evolution, showing viscosity (left) and grain size (right) with isolines at 100 K and 150 K excess temperature. (a) Commonly used viscosity profile [*Steinberger and Calderwood*, 2006] with only diffusion creep (*SC2006* in Table S2). (b,c) Combined diffusion/dislocation rheology, but constant grain size for each mineral phase (*constantGS* in Table S2). (d,e) Evolving grain size and grain size dependent rheology (*reference* in Table S2). (f,g) As in d,e, but a lower diffusion creep activation volume of $V_{\mathrm{diff}} = 1.5 \times 10^{-6}\,\mathrm{m}^3/\mathrm{mol}$ in the lower mantle (*LM-V_{diff}1.5e-6* in Table S2). (h,i) As in f,g, but faster lower mantle grain growth (see Section S2.3; *faster-LM-grain-growth* in Table S2). All parameters can be found in Tables S1 and S2.

displace surrounding material in the upper mantle, also leading to a thickened slab in the lower mantle (Figure 5b).

In models with grain size evolution, two different effects compete: The grain size in subducted slabs is reduced due to strong deformation and slow grain growth at low temperatures, which reduces their viscosity. On the other hand, the low slab temperatures increase their viscosity. As long as slabs are still several hundred degrees colder than the surrounding mantle, temperature has a much stronger influence than grain size and slabs are several orders of magnitude more viscous. However, the feedback between high strain rates, grain size reduction and the implied viscosity reduction leads to low viscosities around slabs – in a similar way as discussed in the previous section for the edges of mantle plumes. This effect allows for fast downward movement of slabs in particular in the upper mantle and transition zone.

Due to the decomposition of ringwoodite to bridgmanite and ferropericlase when slabs enter the lower mantle they have the same small grain size as the surrounding (downwelling) material. This means that the material moving downwards with the slab has a lower viscosity than material that has remained in the lower mantle for a longer time and has had time to grow larger grains. Hence, the mantle around slabs can be deformed more easily, and the highly viscous slabs move faster than in models not considering grain size evolution. The slabs displace the mantle around them instead of deforming internally, leading to the development of large bends (Figure 5c-h) instead of thickening.

This result could also explain why inversions for lateral viscosity variations [*Yang and Gurnis*, 2016] suggest a lower or similar viscosity of subduction zones compared to the surrounding mantle at large scales (~5000 km). Averaged over these large distances, the anomaly of the high-viscosity slab is compensated for by the zone of reduced viscosity surrounding it.

Throughout their evolution in the lower mantle, grains grow more slowly inside of slabs and the grain size difference to the surrounding material therefore becomes larger, while at the same time the temperature difference decreases as the slab begins to thermally equilibrate (Figure S8). This means that over time, the weakening effect of the small grain size becomes more important, and slabs have lower viscosities compared to models without grain size evolution. When they reach the deep mantle, they accumulate as large piles and mix with the surrounding mantle instead of flattening to a layer at the core–mantle boundary.

After some time, the competing effects of grain size and temperature cancel out, and slabs might have the same viscosity as the adjacent mantle despite their lower temperatures.

The more detailed development of slabs is controlled by the parameters used in the creep and grain growth laws. For a low diffusion creep activation volume in the lower mantle, there is almost no vertical viscosity gradient in the lower mantle, but a strong viscosity contrast at 650 km depth. This leads to less bending of the slab in the lower mantle, and a decoupling of the convection in the upper and lower mantle that allows strong lateral displacements between these two layers, leading to sharply bent slabs in the transition zones, and sometimes even to slab break-off (Figure 5e,f). In contrast, a faster grain growth in the lower mantle leads to strong lateral viscosity variations, with low viscosities in regions of downwellings (see Section 3.2). This means an even faster downward movement of slabs, which cross the transition to the lower mantle almost vertically and form a diffuse pile at the core–mantle boundary (Figure 5g,h).

In summary, our models demonstrate that the dynamics of both slabs and plumes is strongly influenced by an evolving grain size, revealing a different and more complex behavior than expected from conventional convection models. As grain size evolution influences both small-scale and large-scale processes, a variety of plume and slab shapes can emerge in dependence of the viscous creep and grain growth parameters.

3.4 Anelastic scaling relationships in the Lower Mantle

We conducted a series of tests to ascertain whether the anelastic relationships of *Jackson and Faul* [2010] calibrated to upper mantle conditions can be extrapolated to the whole mantle. The applicability of these relationships is illustrated by good fits to the 1-D profile shapes (but not everywhere the absolute values) of PREM V_S, V_P and QL6 Q_μ in the upper mantle (Figures 6 and S10). Here we focus on only models with evolving grain size. Shallower than 650 km, we recover excellent fits to global attenuation models when using preferred values of activation volume and relaxation strength ($V^* = 10 \times 10^{-6}$, and $\Delta_B = 1.04$) from *Jackson and Faul* [2010], with the extended Burgers model that includes a low-T peak. Specifically, we obtain a high-Q_μ lid, a low-Q_μ zone just below the lid (akin to models of global asthenosphere), and a roughly constant Q_μ of $\sim$ 150 down to the base of the transition zone. The subtle stepwise increases in Q_μ at the 410 and 520 km discontinuities arise from the change in activation energy at these boundaries. This fine-scale structure is beyond the

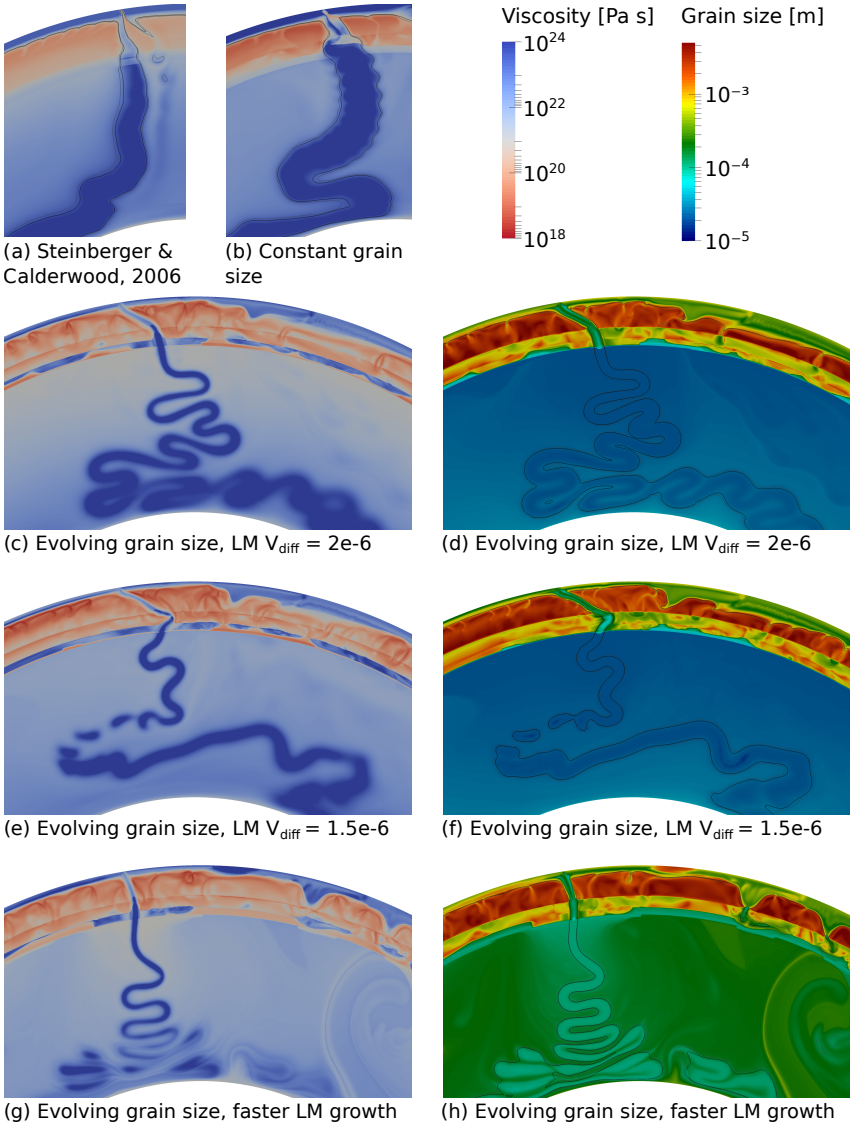

Figure 5. Shape and dynamics of subducting slabs in dependence of grain size evolution, showing viscosity (left) and grain size (right). (a) Commonly used viscosity profile [*Steinberger and Calderwood*, 2006] with only diffusion creep (*SC2006* in Table S2). (b) Combined diffusion/dislocation rheology, but constant grain size for each mineral phase (*constantGS* in Table S2). (c,d) Evolving grain size and grain size dependent rheology (*reference* in Table S2). (e,f) As in c,d, but a lower diffusion creep activation volume of $V_{\text{diff}} = 1.5 \times 10^{-6}$ m^3/mol in the lower mantle (*LM-V_{diff}1.5e-6* in Table S2). (g,h) As in e,f, but faster lower mantle grain growth (see Section S2.3; *faster-LM-grain-growth* in Table S2). All parameters can be found in Tables S1 and S2.

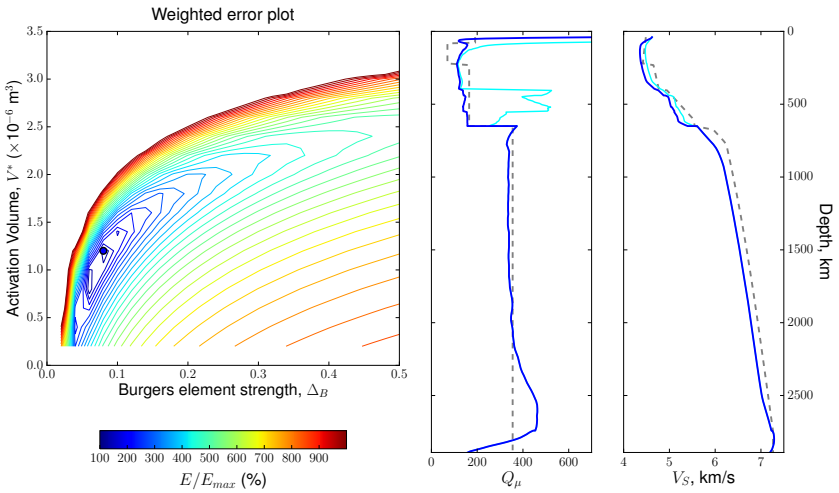

Figure 6. Left: Relative error for comparisons between seismological 1-D models and values predicted using relationships in Section 2.3.4, grid searching through values of lower-mantle Δ_B and V^* for the *faster-LM-grain-growth* model (normalised to 100% at the minimum value). The best fitting (preferred) parameters are $\Delta_B \approx 0.1$ and $V^* \approx 1.0{\times}10^{-6}$ m^3/mol. Right: whole-mantle Q_μ and V_S profiles for the mantle. Blue curve: preferred Δ_B and V^*, with low-T absorption peak in upper mantle, but not in lower mantle; cyan curve: same as blue curve but with no upper mantle absorption peak; dashed grey curves: QL6 Q_μ [*Durek and Ekström*, 1996] and PREM shear velocity, respectively. See Figure S10 for all error maps.

resolution of global Q_μ models at this depth, but is not inconsistent with observations. In this depth range, the three evolving grain size models have negligibly differing 1-D structure.

Q_μ in the deep Earth is poorly constrained, so we seek to reproduce the most well-resolved observations: a sharp increase in Q_μ at the 650 km discontinuity and a roughly constant Q_μ of ~350 throughout the lower mantle [e.g. *Moulik*, 2016; *Widmer et al.*, 1991; *Resovsky et al.*, 2005]. Neither of these conditions is met by extrapolating upper mantle V^* and Δ_B into the lower mantle for any of our models; instead there is is a rapid increase to almost-infinite Q_μ at the base of the transition zone. V^* controls the pressure-dependence of Q_μ, while Δ_B affects its overall scaling and hence the magnitude of the jump at 650 km.

3.4.1 Seismic velocities and the lower mantle absorption peak

Our joint Q_μ and V_S predictions place a constraint on the presence of a low-temperature absorption peak throughout the mantle. This absorption peak (attributed to to elastically-accommodated grain boundary sliding) is required in the upper mantle in order to match attenuation profiles above the transition zone (Figure 6). The upper mantle misfit to QL6 increases by a factor of 3 when the peak is not included, for the *reference* and *faster-LM-grain-growth* models. In the lower mantle, the temperature is sufficiently high that the absorption peak lies above the seismic frequency band (>1 Hz) and does not affect the predicted attenuation; Q_μ can be matched equally well with or without the presence of this peak. However, models including an absorption peak underestimate lower mantle PREM shear velocities systematically, by roughly 2%. This is because total modulus dispersion is a function of the integral of the absorption spectrum from infinite frequency down to the frequency of interest [*Kanamori and Anderson*, 1977; *Minster and Anderson*, 1981; *Takei et al.*, 2014], and so a high frequency peak noticeably decreases lower mantle shear moduli. By comparison to PREM, we therefore rule out the presence of a significant absorption peak beneath the transition zone. For the rest of our analysis, we therefore use a hybrid scaling relationship: above ringwoodite-bridgmanite transition we include a low-T absorption peak, and below this depth we have no peak (Section 3.5).

A small systematic difference between PREM shear velocities is largely due to HeFESTo anharmonic moduli underestimating PREM values (Figure 7). This discrepancy may arise from a) our assumption of a pyrolitic composition throughout, or b) the fact that our models may include higher upper mantle temperatures than the real Earth (we assume a mantle

potential temperature of 1600 K; published values typically range from 1550 – 1670 K, [e.g. *McKenzie et al.*, 2005; *Herzberg et al.*, 2007; *Courtier et al.*, 2007; *Putirka*, 2008]).

3.4.2 Lower mantle anelastic parameters

We grid-search through lower mantle V^* and Δ_B values, computing the weighted misfit to observed $V_S(z)$ from PREM and $Q_\mu(z)$ from QL6 [*Durek and Ekström*, 1996] (Figures 6, S10). $Q_\mu(z)$ misfit in the 600–1000 km depth range is up-weighted by 5× to ensure preferred models capture the well-constrained jump at 650 km. All models qualitatively fit $Q_\mu \sim \infty$ in the lithospheric lid; we do not include misfits from depths shallower than 100 km. Since the goodness of fit to velocity models is contingent on poorly-constrained anharmonic moduli from HeFESTo, as well as assumed temperature and simplified composition (Section 3.4.1), V_S misfit is down-weighted by 2×. In all cases, seismological predictions are computed using the output from the final time step of the dynamic model.

Upper-mantle activation volumes ($V^* \geq 6 \times 10^{-6}$ m^3/mol) produce far too high a gradient in lower-mantle $Q_\mu(z)$. Best fitting lower mantle V^* is $\sim 1.2 \times 10^{-6}$ m^3/mol for all 3 tested models (Table S4). $Q_\mu(z)$ in the Earth is observed to evince negligible, or even negative, gradients with depth [*Resovsky et al.*, 2005; *Widmer et al.*, 1991; *Durek and Ekström*, 1996], requiring a weak pressure dependency of attenuation. Our preferred value of $V^* = 1.2 \times 10^{-6}$ m^3/mol for the *faster-LM-grain-growth* model yields excellent fits to 1-D $V_S(z)$ and $Q_\mu(z)$ profiles (Figure 6). We find that this low value of V^* is primarily controlled by the approximate constancy Q_μ in the lower mantle, and is insensitive to systematic shifts in lower mantle grain size (Figure S9 and Table S4).

It is not possible to replicate the increase in Q_μ at the 650 km discontinuity if there is no corresponding decrease in Δ_B from upper-mantle values (1.04). We find that a reduction in Δ_B to <0.1 achieves the observed step in Q_μ (Table S4). The slightly higher preferred value for the *fast lower mantle grain growth* model ($0.08\ ^{+0.01}_{-0.03}$ versus $0.06\ ^{+0.01}_{-0.03}$ for the *reference* and *LM-V_{diff}1.5e-6* models) arises because of ~3.5× larger grains in the lower mantle compared to other models. We tested the consequence of assuming larger grain size in the lower mantle and found that best fitting Δ_B would increase, from 0.04 to 0.4 as grain size varies from 10^{-5} to 10^{-2} m (Figure S9 and Table S4). By computing equilibrium grain size, we resolve this trade-off, and constrain lower mantle Δ_B. The reduction in Δ_B implies that

for perovskite, the relaxed shear modulus is not much diminished compared to the unrelaxed value.

3.5 Wave speed and Q_μ distributions and heterogeneity spectrum

The full profiles of shear velocity and Q_μ reveal interesting differences between the three models with evolving grain size (Figures 7 and S11). Since each model is contingent on boundary conditions, and does not attempt to simulate the real Earth, here we discuss statistical characteristics of each model and their comparison to Earth models. As expected, there is generally much greater absolute variance in Q_μ than in V_S at all depths in the models, with horizontal perturbations of up to two orders of magnitude for the former standing in contrast to ±5% variations in the latter. For each of these profiles, we use preferred values for Δ_B and V^* (Table S4) to compute lower mantle anelasticity. Since these preferred values are estimated by minimizing misfit to global 1-D Q_μ models, it is no surprise that the average attenuation and velocity profiles look similar between models.

However, interesting distinctions stand out. The *faster-LM-grain growth* model evinces a relatively narrower range of Q_μ values at every depth within the lower mantle than the other two models. This feature reflects the faster growth rates in this model, as small grains within descending slabs more rapidly ripen towards the equilibrium grain size at each depth, despite the cold temperatures.

Both *reference* and *LM-V_{diff}1.5e-6* profiles evince a very broad maximum in Q_μ in the ~1800-2700 km depth range arise from a buildup of incompletely settled cold, high-Q_μ slab material close to the base of the mantle. In the *faster-LM-grain-growth* model, by contrast, this Q_μ maximum is diminished and more confined to deeper depths (~2400-2700 km), reflecting more mature slab settling towards the core-mantle boundary. The faster grain growth accentuates gradients in strain rate (Section 3.3.2), leading to more rapid slab breakup and thermal reworking (Figure 5g,h).

A modest underestimate in Q_μ over the 650-1100 km depth range for the *reference* and *LM-V_{diff}1.5e-6* models results from the inability of models with slow lower mantle grain growth to match simultaneously the increase in Q_μ across the base of the transition zone and the average values of Q_μ in the uppermost lower mantle (Section 3.4).

All three models have very similar average Q_μ profiles in the upper mantle, the histograms show that the *LM-V_{diff}1.5e-6* model has a slightly broader distribution of attenuation values at 120 km depth, for reasons that are not readily apparent. At 1700 km depth, we note that both *reference* and *LM-V_{diff}1.5e-6* models have some subset of negligibly attenuating regions where $1000/Q_\mu \approx 1$. These low attenuation regions do not appear in the *faster-LM-grain-growth* model, because in this model slabs sink down to the core-mantle boundary faster, and slab material accumulates predominantly in the lowermost 500 km of the mantle (see Figure 5).

The velocity profiles are, in aggregate, determined by the temperature structure, which is similar between the three models. Nonetheless, in detail the *faster-LM-grain-growth* model has a larger peak-to-peak velocity heterogeneity than the *reference* and *LM-V_{diff}1.5e-6* models (Figure S11), which have more modest and consistent velocity deviations. This is most pronounced in the lower mantle and might arise from the *faster-LM-grain-growth* model having faster slab descent (so colder temperature minima) coupled with greater mixing (and hence wider temperature gradients). Over longer time scales and accounting for 3-D structure, the differences in rheology between the models (Section 3.2) would likely produce more extensive differences in, for instance, the volume and morphology of subducted material.

4 Discussion

4.1 Geodynamics

We have shown that an evolving grain size that influences mantle rheology has a strong effect on the viscosity structure of the mantle and on the dynamics of mantle convection. In particular, we demonstrate that viscosity variations in the mantle are stronger than expected from models assuming a constant grain size. This result is in contrast to previous studies, which predicted that an evolving grain size would reduce – instead of increase – lateral viscosity variations [*Glišović et al.*, 2015]. Because they infer grain size only from present-day temperatures, they find that regions with high (low) temperatures always feature large (small) grain sizes, which is not necessarily the case in dynamically evolving models (see for example Figure S8).

Our conclusion has notable implications for constraints on mantle viscosities that are based on geodynamic models, and for stirring and mixing of material in the mantle. As the viscosity profiles for the Earth's mantle can be derived from observations only with signifi-

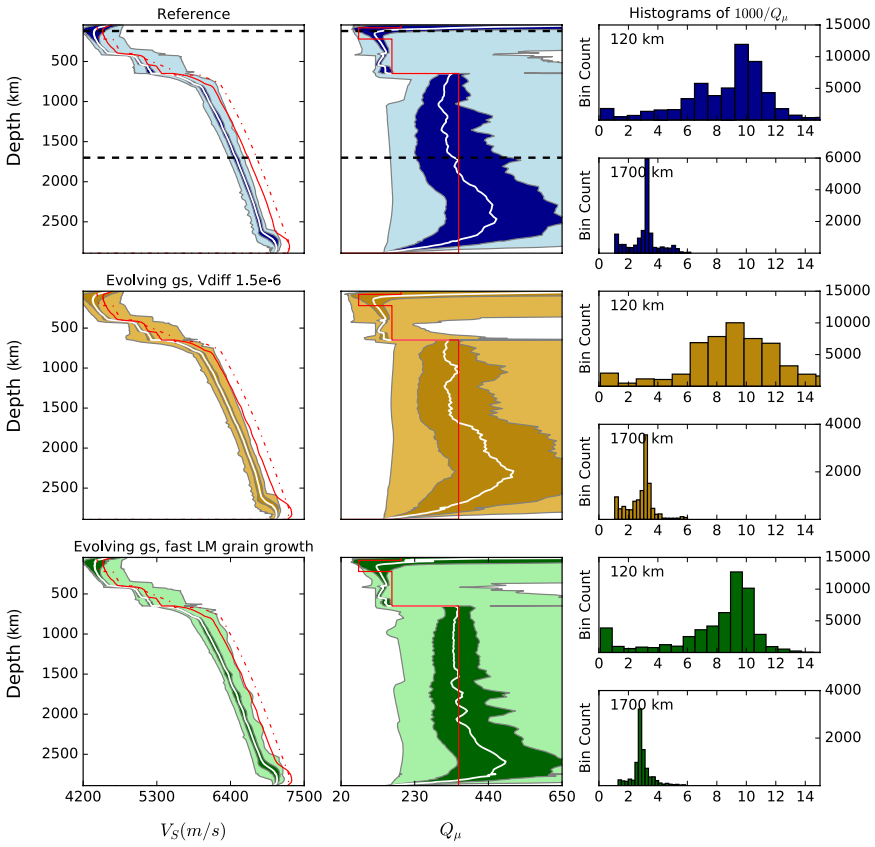

Figure 7. V_S, and Q_μ profiles for three models with evolving grain size, showing one standard deviation about the mean (white) at each depth (darker color) and the maximum/minimum bounds at each depth (lighter color). The estimates of V_S are calculated at 1 Hz while accounting for physical dispersion. Histograms of the distribution of $1000/Q_\mu$ are provided at a depth of 120 km and 1700 km (dashed lines). Values of Q_μ from QL6 (red), anharmonic V_S from HeFESTo (red) and V_S at 1 Hz from PREM (dashed red) are also plotted for comparison.

cant uncertainties, geodynamic modeling studies of subduction zones have been conducted to constrain the viscosity jump between the transition zone and the lower mantle, with an inferred viscosity contrast of approximately 5 – 10 [*Quinteros et al.*, 2010]. If grain size growth is not negligible in the lower mantle, lateral viscosity variations are strong even in the lower mantle, and these estimates are only valid for the location of the subducting slab and its immediate surroundings. However, this region is where the viscosity contrast between upper and lower mantle is smallest: As the amount of downwelling material is much larger than the thermal/chemical anomaly of the slab itself, there is a wide influence zone around the slab where material crosses the 650 km phase transitions and grains are decomposed so that the grain size is small. The viscosity contrast between upper and lower mantle is much higher in regions where material has been in the lower mantle for a longer time (and hence grain sizes are larger), in particular, in our model with fast grain growth in the lower mantle, it is up to a a factor of 50 higher in regions of upwellings (compared to downwellings). This could imply that in some regions, the viscosity contrast between upper and lower mantle is bigger than a factor of 100, up to the point where flow in the upper and lower mantle becomes decoupled, and only plumes and slabs penetrate through this barrier.

The same considerations should be taken into account when inferring lower mantle viscosities from slab sinking speeds. *Cízková et al.* [2012] derive lower mantle depth average viscosities of $3-5\times10^{22}$ Pa s using this method. In our models, however, mantle viscosity surrounding plumes is up to an order higher compared to the viscosity of the mantle around sinking slabs, indicating significantly higher average lower mantle viscosities.

We have shown that grain size reduction due to decomposition reactions, coupled with slow grain growth in cold slabs, results in fine-grained slabs descending through the lower mantle. This phenomenon can substantially weaken slabs that would otherwise have higher viscosity (see Figure 5g,h), and due to the effects of grain size, slabs might have the same viscosity as the adjacent mantle even if they are still 200 K colder (Figure S8). As the smaller grain size in slabs results from lower temperatures (and slower grain growth) over their entire history in the lower mantle, subducted material might even become weaker than the surrounding mantle once it is thermally equilibrated (but while grains are still small). As a consequence of this weakening, slab material could mix into the deep mantle much faster than predicted in conventional mantle convection simulations, and be entrained in mantle plumes more easily.

The effect of grain size on rheology also has implications for the material transport in plumes: Grain size evolution enhances the localization of deformation at the edges of plumes, with relatively uniform velocities in the interior of plume tails, similar to plug flow (and opposed to Poiseuille flow, where the velocity profile is a parabola), so there is only negligible internal deformation in plumes. This means that heterogeneities entrained at the base of the mantle, possibly leading to a chemically zoned plume tail, can be preserved more easily and might be visible in the composition of hot spot tracks at the surface [*Farnetani et al.*, 2012], such as observed for example for Hawaii, Samoa and Marquesas [*Weis et al.*, 2011; *Huang et al.*, 2011].

Our constraints on grain growth parameters offer insights into the stability of antipodal large low shear velocity provinces (LLSVPs), a dominantly long-wavelength (degree 2) feature in the lowermost mantle [e.g. *Dziewonski et al.*, 2010]. While there exists broad consensus on the detection of LLSVPs [e.g. *Lekić et al.*, 2012], their thermo-chemical nature remains a subject of debate [e.g. *Ishii and Tromp*, 1999; *Masters et al.*, 2000; *Davies et al.*, 2012; *French and Romanowicz*, 2015]. If LLSVPs are dense, stable piles in the lowermost mantle, as has been suggested recently [e.g. *Moulik and Ekström*, 2016; *Garnero et al.*, 2016], and have high temperatures, grains in these piles would potentially grow faster than in the average mantle and would have a long time to grow. Assuming that there are no phase transitions present within the piles (due to the high temperatures, which would move the transition from perovskite to post-perovskite to higher pressures than present in the mantle), and that grain pinning does not arise from secondary phases associated with the compositional heterogeneity, this would mean that LLSVPs would also be *large grain size provinces*. In addition to the effect on seismic velocities discussed in Section 4.2.2, this could also affect the stability of these dense piles. Generally, it is assumed that material in the LLSVPs has a much lower viscosity than the surrounding mantle due to its higher temperature. A large grain size could reduce this effect: assuming the same rheologic parameters we used for our geodynamic models, an LLSVP with a temperature excess of 500 K would have a more than 30 times lower viscosity if it had the same grain size as the adjacent mantle. However, after only 50 Ma the viscosity contrast would still be a factor of 20 when assuming the slow grain growth used in the *reference* model, but would only be a factor of 5 for the *faster-LM-grain-growth* parameters. As the viscosity contrast between the pile and the mantle can have a strong effect on entrainment and mixing of material [*Manga*, 1996; *Li and McNamara*,

2013], constraining the grain size within LLSVPs could be an important step for modeling the development and evolution of heterogeneities in the mantle.

4.2 Seismology

4.2.1 Extrapolation to lower mantle conditions

Laboratory limitations preclude deformation experiments at lower mantle conditions. The parameters which circumscribe deep mantle anelasticity are unknown from direct experimental data and poorly constrained by geodynamic models. Our ability to produce reasonable predictions for lower mantle attenuation provides indirect evidence for the ubiquity of a broadband HTB absorption band [e.g., *Cooper*, 2002; *Jackson and Faul*, 2010; *McCarthy et al.*, 2011; *McMillan et al.*, 2003]. Our results also suggest that the high-pressure phase assemblage of the lower mantle has a proportionally higher relaxed modulus than upper mantle rocks (lower Δ_B) and lower activation volume (V^*). If the lower mantle Q_μ were greater (lower) than QL6 [e.g. *Hwang and Ritsema*, 2011], we would recover similar V^* but a slightly higher (lower) Δ_B in the lower mantle; substantial contrast with the upper mantle values would persist.

A drop in V^* across the upper–lower mantle boundary is predicted on purely theoretical grounds [*Sammis et al.*, 1977] and is independently supported by satellite observations [*Ivins et al.*, 1993]. Our estimate of V^* places quantitative bounds on the thermodynamic parameter V_{diff} that is key to geodynamic modeling, assuming the dominance of diffusionally accommodated anelastic processes. Note that the $V^* \sim 1.2 \times 10^{-6}$ m^3/mol we obtain from seismological arguments agrees well with the $V_{\text{diff}} = 1.5 \times 10^{-6}$ m^3/mol used in our dynamical model that achieved the most realistic depth dependence of viscosity [cf. *Steinberger and Calderwood*, 2006]. We model a constant V^*, but in fact it is likely to decrease with increasing pressure in the lower mantle [*Poirier and Liebermann*, 1984]. Our constant value can be taken as an average across that pressure range. The effect of incorporating a lower mantle negative gradient in V^* would be to reduce the increase in viscosity (and Q_μ) with depth.

We find that the *faster-LM-grain-growth* provides marginally better overall fits than the *reference* model (Figure S11 and errors in Table S4). The slower grain growth in the *reference* model results in ~3.5× smaller grain size throughout the lower mantle. Since the grain sizes are so small, no value of V^* can offset the pressure dependency of attenuation without resulting in smaller-than-observed Q_μ in the mid-lower mantle. While the difference in over-

all weighted fits is not statistically significant, our results hint that faster lower mantle grain growth is more easily compatible with observed seismic parameters, and supports our revised assessment of experimental high-pressure grain growth rate data (Section 2.2).

Our models show that due to the significant changes of rheologic and grain growth parameters across phase transitions, phase regions in the mantle transition zone can be dominated by one deformation mechanism. With the input parameters used in our study, the wadsleyite phase region primarily deforms by dislocation creep (Figure 3), with potential implications for producing transition zone seismic anisotropy through a crystallographic preferred orientation that results from time-integrated deformation.

We have argued that a high frequency absorption peak does not apply in the lower mantle. The experimentally observed relaxation strength for olivine due to elastically accommodated grain boundary sliding is small. Since our modeling indicates that the relaxation strength of the absorption band (Δ_B) for bridgmanite is much smaller than for olivine, it is consistent that the relaxation due to elastically accommodated grain boundary sliding (putatively Δ_P) should also be negligible for the lower mantle.

In each of the models with evolving grain size, we observe a buildup of cold, high-Q_μ slab material in the lower ~1000 km of the mantle. Although our models ran for limited model time, this feature may represent an equilibrium state. While several 1-D mantle attenuation models (including QL6, used to optimize our lower mantle fitting parameters) show roughly constant lower-mantle Q_μ [e.g. *Moulik*, 2016; *Widmer et al.*, 1991; *Resovsky et al.*, 2005], others include a broad Q_μ maximum in the lowermost mantle [*Hwang and Ritsema*, 2011; *Lawrence and Wysession*, 2006]. Our work provides a potential explanation for this high-Q_μ region as a slab "graveyard" in the lowermost mantle.

4.2.2 Do we underestimate thermal gradients from seismic tomography?

Seismological observations provide the most detailed proxy measurements of the Earth's interior physical state. Community efforts to map the 3-D velocity and attenuation structure of Earth's mantle have the explicit goal of elucidating temperature and composition, for comparison with other geophysical and geochemical constraints. However, grain size variations disrupt one-to-one mapping from imaged velocities to inferred temperatures [*Karato*, 1993]. The assumption of grain size constancy can lead to systematic misinterpretation of velocities if grain size is – as we have demonstrated – related to temperature.

Our models show that, in general, slabs are cold and consequently have slow grain growth and smaller grains. Their lower temperature results in higher anharmonic velocities compared to their surroundings, but their small grains accentuate the anelastic effects, slightly depressing effective wave speeds. The net effect is that the slab is only moderately faster than its surroundings. Typically, a moderately fast velocity is inferred to reflect a moderately cold slab. However, this would be an underestimate of its thermal state; the slab is in fact substantially cooler then its surroundings but the grain size buffers the temperature effect. Our calculations show that using an constant average grainsize in the upper mantle would lead to discrepancies of up to 2% in $\Delta V_S/V_S$ (Figure 8).

The opposite argument works for plumes. Since plumes have high temperatures but large grains, a simple mapping from velocity to temperature would understate their true temperature excess. However, since the differential plume temperatures compared to their surroundings, the effects are lesser ($< 0.5\%\Delta V_S/V_S$ in our model). In Figure 8, we used the 'true' median model grain size for the upper mantle ($\sim$ 1.43 mm) for the constant grain size comparison. If one were to use an wholly inappropriate grain size when interpreting observed velocity heterogeneity, the systematic over-/under-estimate of temperature variation would likely be even greater than the discrepancies shown here.

The overall consequence is that global seismic models will have a smaller range in velocities than would be the case without grain size variation. Standard interpretations of velocities in terms of temperature alone omit the substantial contributions from grain size. The implication is that we may have to re-evaluate the true range of temperature heterogeneity in the Earth's mantle, especially in regions with strong variations in grain size and temperature. This effect could be less important in the mid-mantle since the overall attenuation is low (high Q_μ), such that the additional effect of grain size does not contribute substantially to the variation in seismic velocities.

This conclusion is important in the context of discussions about the temperature anomaly associated with LLSVPs. Given seismic data coverage, previous workers have suggested that the ~2.5% slow $\delta V_S/V_S$ [*e.g.*, *Ritsema et al.*, 1999; *Moulik and Ekström*, 2014; *French and Romanowicz*, 2014] in these structures implies a 1000 K [*Schuberth et al.*, 2009] thermal contrast to ambient mantle. Absent grain size differences, for this temperature anelastic processes would reduce LLSVP Q_μ to ~90 (from ~360), lowering V_S in these structures by a further 1.0% compared to ambient mantle. Large grains grown within long-lived LLSVPs

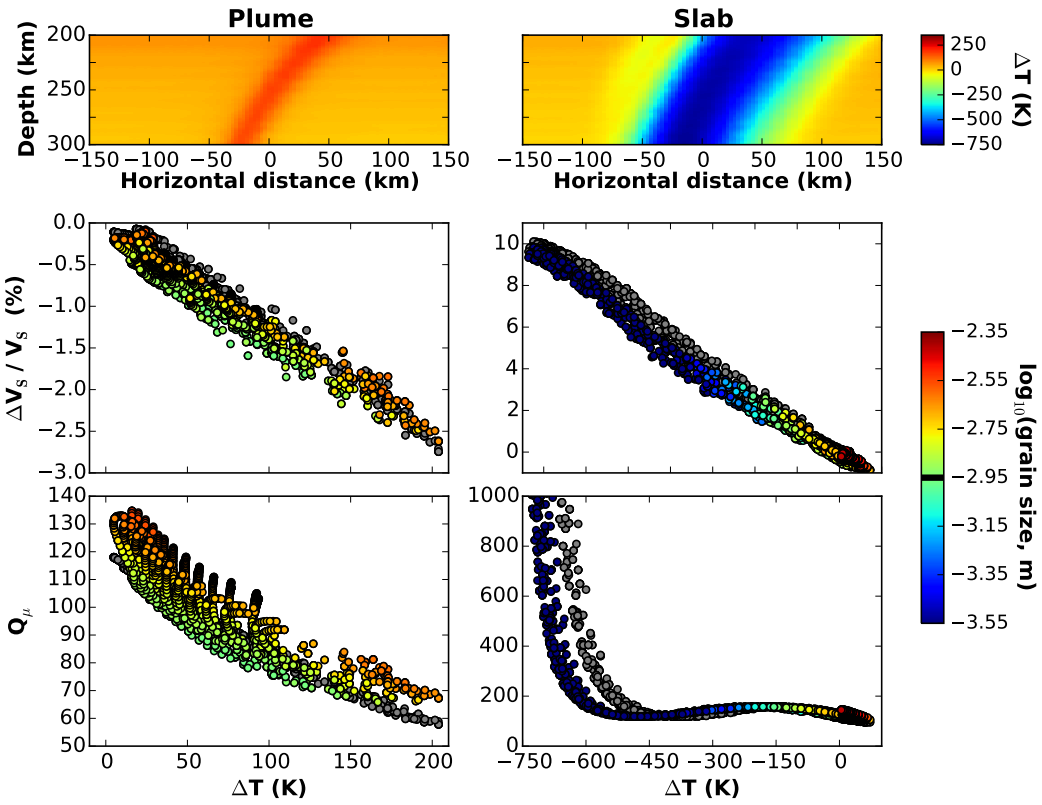

Figure 8. Shear velocity and attenuation in extreme temperature regions of the upper mantle, accounting for grain size. Top panels: differential temperature (ΔT) field (relative to average at each depth) in a thin slice through a plume (left) and a slab (right) in the *faster-LM-grain-growth* model. Middle panels: differential V_S (relative to model average at that depth) against ΔT for the same region assuming constant upper mantle grain size of 1.43×10^{-3} m (grey points and black line on scale bar) contrasted with variable grain size computed in the model (colored points). Bottom panels: Q_μ against ΔT for the same set of points.

(Section 4.1) would markedly buffer the effect of temperature on velocity: two orders of magnitude larger grains would offset approximately 250K of excess temperature. In this case, these structures could be hotter than previously considered, requiring even greater compositional density to stabilize them against convection on long timescales [*Moulik and Ekström*, 2016; *Garnero et al.*, 2016, and references therein]. On the other hand, the "ultra low velocity zones" [*McNamara et al.*, 2010] at the margins of LLSVPs may be particularly slow because they contain small grains due to high strain rates and localized deformation at the boundary of the high-viscosity LLSVPs.

4.3 Uncertainties

There are different sources of uncertainties in our models: The rheology and grain growth parameters (see Section S6.1), the geodynamic model assumptions (see Section S6.2), and the seismological parameterizations (see Section S6.3). Experimentally derived rheological and grain growth parameters relevant to the mantle have large uncertainties, in part because of the difficulty of conducting deformation experiments at high pressures and partly because of the large extrapolation in strain rate between experiments and the Earth. In addition, variations in chemistry cause changes in both rheology and grain size parameters. These uncertainties in the experimental data also limit the interpretation of our geodynamic models. As the model complexity made a comprehensive search of the parameter space infeasible, and we only study thermal (as opposed to thermo-chemical) convection, our predictions for the influence of grain size evolution on the dynamics of the Earth's mantle remain mainly qualitative. In addition, we have made a number of assumptions in extrapolating laboratory results to the Earth, in particular assuming that the constitutive form of the anelastic scaling relationship holds throughout the mantle. However, despite our relatively simplistic approach, we obtain good qualitative fits to upper mantle velocity and attenuation profiles, and highly reasonable fits to robust aspects of lower mantle Q_μ structure, consistent with prior mineralogical expectations and dynamical constraints.

5 Conclusions and Outlook

We have studied the influence of grain size evolution on mantle dynamics, seismic velocities and attenuation, using available constraints from mineral physics. Feedback between seismology and geodynamics is used to iteratively improve both modeling schemes in a self-consistent fashion. Our models demonstrate that an evolving grain size drastically affects the

dynamics of mantle convection and the viscosity structure of the mantle, and is important for the shape of upwellings and downwellings. Predicting seismically observed parameters from the output of geodynamic models allows us to resolve trade-offs between temperature and grain size in controlling the anelastic behavior of rocks. Our key findings inform the thermo-chemical interpretations of several seismically observed features in the Earth's mantle:

Dynamically evolving grain size in mantle convection models leads to strong lateral viscosity contrasts in the mantle. In the upper mantle, lateral viscosity variations of six orders of magnitude result from grain size alone. In the lower mantle, grain size is controlled by how long material has resided there, and viscosity contrasts between "old" and "young" material of the same temperature can easily reach an order of magnitude.

Positive feedback between grain size reduction and viscosity reduction results in shear localization, for example at the edges of mantle plumes and in a low-viscosity layer at the base of the lithosphere. Hence, viscosity at the edges of thermal plumes is lower than within, despite lower temperatures. As a consequence, the velocity in the interior of the plume is relatively uniform, suggesting only minimal mixing of material.

Low temperatures and high stresses in and near to slabs result in small grain sizes, which lead to higher seismic attenuation (lower Q_μ) than expected, and make slabs weaker than predicted in conventional mantle convection models. Slab material can have the same viscosity as the surrounding mantle despite lower temperatures, and mixing is faster than in models without grain size evolution.

Lower mantle seismic observations place constraints on physical properties not yet constrained by high-pressure experiments. We find support for a lower activation volume ($V^* \sim 10^{-6}$ m^3/mol) and relaxation strength ($\Delta_B < 0.1$) in the lower mantle. Preferred lower mantle activation volumes obtained independently from geodynamical (1.5e-6 m^3/mol) and seismological (1.2e-6 m^3/mol) considerations agree extremely well, corroborating ideas about diffusional processes at high pressure. The model with *faster-LM-grain-growth* provided the best qualitative fits to globally averaged 1-D velocity and attenuation profiles, supporting geodynamic arguments for faster growth rates in the lower mantle.

An anelastic treatment of seismic observables provides an additional tool to analyze and quantitatively compare geodynamic models. We have generated velocity and shear attenuation maps from the geodynamic model outputs, enabling statistical comparisons of

the models. In the lower mantle, the *faster-LM-grain-growth* has a smaller range of Q_μ and larger high-δV_S regions of than models with slow grain growth, likely because of the smaller lag times for grain size evolution. The thermal gradients in the upper mantle inferred from seismic tomography are potentially underestimated in regions with strong thermal and grain size variations (e.g. plumes, slabs).

Acknowledgments

All authors contributed equally to the conception and development of this work and are therefore listed alphabetically. This material is based on work started during the 2014 Cooperative Institute of Dynamic Earth Research (CIDER) summer program at the Kavli Institute of Theoretical Physics at the University of California at Santa Barbara. The CIDER program is supported by the National Science Foundation (NSF) Frontiers of Earth Systems Dynamics grant EAR-1135452. P.M. wishes to acknowledge support from the NSF through the grants EAR-08-38093, EAR-13-15984 and EAR-13-45082. J.D. and R.G. were partially supported by the Computational Infrastructure for Geodynamics initiative (CIG), through the NSF under Awards No. EAR-0949446 and EAR-1550901, administered by The University of California-Davis, and the NSF under award OCI-1148116 as part of the Software Infrastructure for Sustained Innovation (SI2) program. J.D. acknowledges the support of the Helmholtz graduate research school GeoSim. The computational resources for the geodynamic models were provided by the North-German Supercomputing Alliance (HLRN) as part of the project "Plume-Plate interaction in 3D mantle flow – Revealing the role of internal plume dynamics on global hot spot volcanism". U.F. acknowledges support from NSF grant EAR-1321889 and EAR-1464024. The geodynamic models were computed with the open-source software ASPECT (*http://aspect.dealii.org*) and visualized with the open-source program ParaView (*http://www.paraview.org*). The necessary settings to reproduce the models are included in the supplementary material.

References

Abers, G. A., K. Fischer, G. Hirth, D. Wiens, T. Plank, B. K. Holtzman, C. McCarthy, and E. Gazel (2014), Reconciling mantle attenuation-temperature relationships from seismology, petrology, and laboratory measurements, *Geochemistry, Geophysics, Geosystems*, *15*(9), 3521–3542.

1063 Aizawa, Y., A. Barnhoorn, U. H. Faul, J. D. F. Gerald, I. Jackson, and I. Kovács (2008), Seis-
1064 mic Properties of Anita Bay Dunite: an Exploratory Study of the Influence of Water, *Jour-*
1065 *nal of Petrology*, *49*(4), 841–855.

1066 Anderson, D. L., and J. B. Minster (1979), The frequency dependence of Q in the Earth and
1067 implications for mantle rheology and Chandler wobble, *Geophysical Journal Interna-*
1068 *tional*, *58*(2), 431–440.

1069 Anderson, D. L., and J. B. Minster (1981), The physics of creep and attenuation in the man-
1070 tle, *Anelasticity in the Earth*, *4*, 5–11.

1071 Ardell, A. (1972), On the coarsening of grain boundary precipitates, *Acta Metallurgica*,
1072 *20*(4), 601–609, doi:http://dx.doi.org/10.1016/0001-6160(72)90015-6.

1073 Austin, N. J., and B. Evans (2007), Paleowattmeters: A scaling relation for dynamically re-
1074 crystallized grain size, *Geology*, *35*, 343, doi:10.1130/G23244A.1.

1075 Ave Lallemant, H. G., J.-C. C. Mercier, N. L. Carter, and J. V. Ross (1980), Rheology of
1076 the upper mantle: Inferences from peridotite xenoliths, *Tectonophysics*, *70*, 85–113, doi:
1077 10.1016/0040-1951(80)90022-0.

1078 Bangerth, W., J. Dannberg, R. Gassmöller, T. Heister, et al. (2017), ASPECT: Advanced
1079 Solver for Problems in Earth's ConvecTion, User Manual, doi:10.6084/m9.figshare.
1080 4865333.

1081 Barnhoorn, A., I. Jackson, J. D. Fitz Gerald, A. Kishimoto, and K. Itatani (2016), Grain size-
1082 sensitive viscoelastic relaxation and seismic properties of polycrystalline MgO, *Journal of*
1083 *Geophysical Research*, *121*(7), 4955–4976.

1084 Becker, T. W., B. Kustowski, and G. Ekström (2008), Radial seismic anisotropy as a con-
1085 straint for upper mantle rheology, *Earth and Planetary Science Letters*, *267*(1), 213–227.

1086 Behn, M. D., G. Hirth, and J. R. Elsenbeck II (2009), Implications of grain size evolution on
1087 the seismic structure of the oceanic upper mantle, *Earth and Planetary Science Letters*,
1088 *282*(1-4), 178–189.

1089 Bercovici, D., and Y. Ricard (2014), Plate tectonics, damage and inheritance, *Nature*, *508*,
1090 513–516, doi:10.1038/nature13072.

1091 Boehler, R. (2000), High-pressure experiments and the phase diagram of lower mantle and
1092 core materials, *Reviews of Geophysics*, *38*(2), 221–245.

1093 Bower, D. J., M. Gurnis, and M. Seton (2013), Lower mantle structure from paleogeograph-
1094 ically constrained dynamic earth models, *Geochemistry, Geophysics, Geosystems*, *14*(1),
1095 44–63.

Burke, J. E. (1949), *Grain control in industrial metallurgy*, American Society for Metals.

Christensen, U. R., and A. W. Hofmann (1994), Segregation of subducted oceanic crust in the convecting mantle, *Journal of Geophysical Research: Solid Earth*, *99*(B10), 19,867–19,884.

Cízková, H., A. P. van den Berg, W. Spakman, and C. Matyska (2012), The viscosity of earth's lower mantle inferred from sinking speed of subducted lithosphere, *Physics of the earth and Planetary Interiors*, *200*, 56–62.

Cooper, R. F. (2002), Seismic Wave Attenuation: Energy Dissipation in Viscoelastic Crystalline Solids, *Reviews in Mineralogy and Geochemistry*, *51*(1), 253–290.

Courtier, A. M., M. G. Jackson, J. F. Lawrence, Z. Wang, C.-T. A. Lee, R. Halama, J. M. Warren, R. Workman, W. Xu, M. M. Hirschmann, et al. (2007), Correlation of seismic and petrologic thermometers suggests deep thermal anomalies beneath hotspots, *Earth and Planetary Science Letters*, *264*(1), 308–316.

Crowley, J. W., M. Gérault, and R. J. O'Connell (2011), On the relative influence of heat and water transport on planetary dynamics, *Earth and Planetary Science Letters*, *310*(3-4), 380–388.

Dannberg, J., and S. V. Sobolev (2015), Low-buoyancy thermochemical plumes resolve controversy of classical mantle plume concept, *Nature communications*, *6*, doi:10.1038/ncomms7960.

Davies, D. R., S. Goes, J. H. Davies, B. S. A. Schuberth, H. P. Bunge, and J. Ritsema (2012), Reconciling dynamic and seismic models of Earth's lower mantle: The dominant role of thermal heterogeneity, *Earth Planet. Sci. Lett.*, *353-354*, 253–269.

Drury, M. R., and J. D. Fitz Gerald (1998), Mantle Rheology: Insights from Laboratory Studies of Deformation and Phase Transition, in *The Earth's Mantle*, edited by I. Jackson, pp. 503–560, Cambridge University Press, doi:10.1017/CBO9780511573101.014, Cambridge Books Online.

Durand, S., J. Matas, S. Ford, Y. Ricard, B. Romanowicz, and J. P. Montagner (2013), Insights from ScS–S measurements on deep mantle attenuation, *Earth and Planetary Science Letters*, *374*(C), 101–110.

Durek, J. J., and G. Ekström (1996), A radial model of anelasticity consistent with long-period surface-wave attenuation, *Bulletin of the Seismological Society of America*, *86*(1A), 144–158.

1128 Dziewonski, A. M., and D. L. Anderson (1981), Preliminary reference Earth model, *Physics*
1129 *Of The Earth And Planetary Interiors*, *25*(4), 297–356.

1130 Dziewonski, A. M., V. Lekic, and B. A. Romanowicz (2010), Mantle Anchor Structure: An
1131 argument for bottom up tectonics, *Earth Planet. Sci. Lett.*, *299*, 69–79.

1132 Farnetani, C. (1997), Excess temperature of mantle plumes: The role of chemical stratifica-
1133 tion across D", *Geophysical Research Letters*, *24*(13), 1583–1586.

1134 Farnetani, C. G., A. W. Hofmann, and C. Class (2012), How double volcanic chains sample
1135 geochemical anomalies from the lowermost mantle, *Earth and Planetary Science Letters*,
1136 *359*, 240–247.

1137 Faul, U., and I. Jackson (2015), Transient creep and strain energy dissipation: An experimen-
1138 tal perspective, *Annual Review of Earth and Planetary Sciences*, *43*, 541–569.

1139 Faul, U. H., and I. Jackson (2005), The seismological signature of temperature and grain size
1140 variations in the upper mantle, *Earth Planet. Sci. Lett.*, *234*(1–2), 119–134, doi:http://dx.
1141 doi.org/10.1016/j.epsl.2005.02.008.

1142 Faul, U. H., and I. Jackson (2007), Diffusion creep of dry, melt-free olivine, *Journal of Geo-*
1143 *physical Research (Solid Earth)*, *112*, B04204, doi:10.1029/2006JB004586.

1144 Faul, U. H., and I. Jackson (2015), Transient creep and strain energy dissipation, *Ann. Rev.*
1145 *Earth Planet. Sci.*, *43*(1), 541–569, doi:10.1146/annurev-earth-060313-054732.

1146 Fei, H., M. Wiedenbeck, D. Yamazaki, and T. Katsura (2013), Small effect of water on
1147 upper-mantle rheology based on silicon self-diffusion coefficients, *Nature*, *498*, 213–215,
1148 doi:10.1038/nature12193.

1149 Ford, H. A., K. M. Fischer, and V. Lekic (2014), Localized shear in the deep lithosphere be-
1150 neath the san andreas fault system, *Geology*, *42*(4), 295–298, doi:10.1130/G35128.1.

1151 French, S. W., and B. Romanowicz (2015), Broad plumes rooted at the base of the Earth's
1152 mantle beneath major hotspots, *Nature*, *525*(7567), 95–99.

1153 French, S. W., and B. A. Romanowicz (2014), Whole-mantle radially anisotropic shear ve-
1154 locity structure from spectral-element waveform tomography, *Geophysical Journal Inter-*
1155 *national*, *199*, 1303–1327.

1156 Frost, H. J., and M. F. Ashby (1982), *Deformation-mechanism maps: The plasticity and*
1157 *creep of metals and ceramics*, Pergamon Press, Oxford, UK.

1158 Garapić, G., U. H. Faul, and E. Brisson (2013), High-resolution imaging of the melt distri-
1159 bution in partially molten upper mantle rocks: evidence for wetted two-grain boundaries,
1160 *Geochemistry, Geophysics, Geosystems*, *14*(3), 556–566.

1161 Garnero, E. J., A. K. McNamara, and S.-H. Shim (2016), Continent-sized anomalous zones
1162 with low seismic velocity at the base of Earth's mantle, *Nature*, *9*, 481–489.
1163 Gerya, T. V., L. L. Perchuk, W. V. Maresch, and A. P. Willner (2004), Inherent gravitational
1164 instability of hot continental crust: Implications for doming and diapirism in granulite
1165 facies terrains, *Geological Society of America Special Papers*, *380*, 97–115.
1166 Glišović, P., A. M. Forte, and M. W. Ammann (2015), Variations in grain size and vis-
1167 cosity based on vacancy diffusion in minerals, seismic tomography, and geodynami-
1168 cally inferred mantle rheology, *Geophysical Research Letters*, *42*(15), 6278–6286, doi:
1169 10.1002/2015GL065142, 2015GL065142.
1170 Goetze, C. (1977), Bounds on the subsolidus attenuation for four rock types at simultane-
1171 ous high temperature and pressure, *Tectonophysics*, *42*, 1, doi:10.1016/0040-1951(77)
1172 90018-X.
1173 Gribb, T. T., and R. F. Cooper (1998), Low-frequency shear attenuation in polycrystalline
1174 olivine: Grain boundary diffusion and the physical significance of the Andrade model for
1175 viscoelastic rheology, *Journal of Geophysical Research*, *103*(B11), 27,267–27,279.
1176 Guermond, J.-L., R. Pasquetti, and B. Popov (2011), Entropy viscosity method for nonlinear
1177 conservation laws, *Journal of Computational Physics*, *230*(11), 4248–4267.
1178 Gurnis, M., M. Turner, S. Zahirovic, L. DiCaprio, S. Spasojevic, R. D. Müller, J. Boyden,
1179 M. Seton, V. C. Manea, and D. J. Bower (2012), Plate tectonic reconstructions with con-
1180 tinuously closing plates, *Computers & Geosciences*, *38*(1), 35–42.
1181 Hall, C. E., and E. M. Parmentier (2003), Influence of grain size evolution on convective
1182 instability, *Geochem. Geophys. Geosyst.*, *4*, 1029, doi:10.1029/2002GC000308.
1183 Hammond, W. C., and E. D. Humphreys (2000), Upper mantle seismic wave attenuation:
1184 Effects of realistic partial melt distribution, *Journal of Geophysical Research*, *105*(B5),
1185 10,987–10,999.
1186 Hernlund, J. W., C. Thomas, and P. J. Tackley (2005), A doubling of the post-perovskite
1187 phase boundary and structure of the Earth's lowermost mantle, *Nature*, *434*(7035), 882–
1188 886.
1189 Herzberg, C., and E. Gazel (2009), Petrological evidence for secular cooling in mantle
1190 plumes, *Nature*, *458*, 619–622.
1191 Herzberg, C., P. D. Asimow, N. Arndt, Y. Niu, C. Lesher, J. Fitton, M. Cheadle, and A. Saun-
1192 ders (2007), Temperatures in ambient mantle and plumes: Constraints from basalts, pi-
1193 crites, and komatiites, *Geochemistry, Geophysics, Geosystems*, *8*(2).

1194 Hiraga, T., C. Tachibana, N. Ohashi, and S. Sano (2010), Grain growth systematics for
1195 forsterite +/- enstatite aggregates: Effect of lithology on grain size in the upper mantle,
1196 *Earth and Planetary Science Letters*, *291*, 10–20, doi:10.1016/j.epsl.2009.12.026.
1197 Hirschmann, M. M. (2006), Water, melting, and the deep Earth H2O cycle, *Annu. Rev. Earth*
1198 *Planet. Sci.*, *34*(1), 629–653.
1199 Hirth, G., and D. Kohlstedt (2003), Rheology of the upper mantle and the mantle wedge: A
1200 view from the experimentalists, *Washington DC American Geophysical Union Geophysi-*
1201 *cal Monograph Series*, *138*, 83–105, doi:10.1029/138GM06.
1202 Hirth, G., and D. L. Kohlstedt (1996), Water in the oceanic upper mantle: Implications for
1203 rheology, melt extraction and the evolution of the lithosphere, *Earth and Planetary Sci-*
1204 *ence Letters*, *144*(1-2), 93–108.
1205 Holtzman, B. K. (2016), Questions on the existence, persistence, and mechanical effects of
1206 a very small melt fraction in the asthenosphere, *Geochemistry, Geophysics, Geosystems*,
1207 *17*(2), 470–484.
1208 Huang, S., P. S. Hall, and M. G. Jackson (2011), Geochemical zoning of volcanic chains as-
1209 sociated with pacific hotspots, *Nature Geoscience*, *4*(12), 874–878.
1210 Hwang, Y. K., and J. Ritsema (2011), Earth and Planetary Science Letters, *Earth and Plane-*
1211 *tary Science Letters*, *303*(3-4), 369–375.
1212 Ishii, M., and J. Tromp (1999), Normal-mode and free-air gravity constraints on lateral varia-
1213 tions in velocity and density of Earth's mantle, *Science*, *285*, 1231–1236.
1214 Ito, E., and H. Sato (1991), Aseismicity in the lower mantle by superplasticity of the de-
1215 scending slab, *Nature*, *351*, 140, doi:10.1038/351140a0.
1216 Ito, G. (2001), Reykjanes 'V'-shaped ridges originating from a pulsing and dehydrating man-
1217 tle plume, *Nature*, *411*(6838), 681.
1218 Ivins, E. R., C. G. Sammis, and C. F. Yoder (1993), Deep mantle viscous structure with prior
1219 estimate and satellite constraint, *Journal of Geophysical Research: Solid Earth*, *98*(B3),
1220 4579–4609, doi:10.1029/92JB02728.
1221 Jackson, I., and U. H. Faul (2010), Grainsize-sensitive viscoelastic relaxation in olivine: To-
1222 wards a robust laboratory-based model for seismological application, *Phys. Earth Planet.*
1223 *Int.*, *183*, 151–163, doi:10.1016/j.pepi.2010.09.005.
1224 Jackson, I., M. S. Paterson, and J. D. F. Gerald (1992), Seismic wave dispersion and atten-
1225 uation in Åheim dunite: an experimental study, *Geophysical Journal Interational*, *108*,
1226 517–534.

1227 Jackson, I., F. Gerald, D. John, U. H. Faul, and B. H. Tan (2002), Grain-size-sensitive seis-
1228 mic wave attenuation in polycrystalline olivine, *Journal of Geophysical Research: Solid*
1229 *Earth*, *107*(B12).

1230 Jackson, I., U. H. Faul, J. D. Fitz Gerald, and B. H. Tan (2004), Shear wave attenuation and
1231 dispersion in melt-bearing olivine polycrystals: 1. Specimen fabrication and mechanical
1232 testing, *Journal of Geophysical Research*, *109*(B6), B06,201.

1233 Jaroslow, G. E., G. Hirth, and H. J. B. Dick (1996), Abyssal peridotite mylonites: impli-
1234 cations for grain-size sensitive flow and strain localization in the oceanic lithosphere,
1235 *Tectonophysics*, *256*, 17–37, doi:10.1016/0040-1951(95)00163-8.

1236 Jaupart, C., S. Labrosse, F. Lucazeau, and J. C. Mareschal (2015), Temperatures, Heat and
1237 Energy in the Mantle of the Earth, in *Treatise on Geophysics*, vol. 7, edited by G. Schu-
1238 bert, 2 ed., chap. 7, pp. 223–270, Elsevier, Oxford, doi:10.1016/B978-044452748-6.
1239 00114-0.

1240 Jones, S., B. Murton, J. Fitton, N. White, J. Maclennan, and R. Walters (2014), A joint
1241 geochemical–geophysical record of time-dependent mantle convection south of Iceland,
1242 *Earth and Planetary Science Letters*, *386*, 86–97, doi:http://dx.doi.org/10.1016/j.epsl.
1243 2013.09.029.

1244 Kanamori, H., and D. L. Anderson (1977), Importance of physical dispersion in surface wave
1245 and free oscillation problems: Review, *Reviews of Geophysics*, *15*(1), 105–112.

1246 Karato, S. (1989), Grain growth kinetics in olivine aggregates, *Tectonophysics*, *168*, 255–
1247 273.

1248 Karato, S., and H. A. Spetzler (1990), Defect microdynamics in minerals and solid state
1249 mechanisms of seismic wave attenuation and velocity dispersion in the mantle, *Reviews*
1250 *of Geophysics*, *28*, 399–421, doi:10.1029/RG028i004p00399.

1251 Karato, S.-i. (1993), Importance of anelasticity in the interpretation of seismic tomography,
1252 *Geophysical Research Letters*, *20*(15), 1623–1626.

1253 Karato, S.-I. (1997), Phase transformations and rheological properties of mantle minerals,
1254 in *Earth's Deep Interior*, vol. 7, edited by D. Crossley, pp. 223–272, Gordon and Breach,
1255 London.

1256 Karato, S.-I., M. S. Paterson, and J. D. Fitzgerald (1986), Rheology of synthetic olivine
1257 aggregates - Influence of grain size and water, *J. Geophys. Res.*, *91*, 8151–8176, doi:
1258 10.1029/JB091iB08p08151.

Karato, S.-i., M. R. Riedel, and D. A. Yuen (2001), Rheological structure and deformation of subducted slabs in the mantle transition zone: implications for mantle circulation and deep earthquakes, *Physics of the Earth and Planetary Interiors*, *127*, 83–108, doi:10.1016/S0031-9201(01)00223-0.

Kawazoe, T., Y. Nishihara, T. Ohuchi, N. Miyajima, G. Maruyama, Y. Higo, K. ichi Funakoshi, and T. Irifune (2016), Creep strength of ringwoodite measured at pressureâĂŞtemperature conditions of the lower part of the mantle transition zone using a deformationâĂŞDIA apparatus, *Earth and Planetary Science Letters*, *454*, 10–19, doi:10.1016/j.epsl.2016.08.011.

Korenaga, J. (2005), Firm mantle plumes and the nature of the core mantle boundary region, *Earth Planet. Sci. Lett.*, *232*, 29–37, doi:10.1016/j.epsl.2005.01.016.

Kronbichler, M., T. Heister, and W. Bangerth (2012), High accuracy mantle convection simulation through modern numerical methods, *Geophysical Journal International*, *191*, 12–29, doi:10.1111/j.1365-246X.2012.05609.x.

Kurat, G., G. Niedermayr, and M. Prinz (1982), Peridot von Zabargad, Rotes Meer, *Der Aufschluss*, *33*, 169–182.

Lawrence, J. F., and M. E. Wysession (2006), QLM9: A new radial quality factor (Qμ) model for the lower mantle, *Earth and Planetary Science Letters*, *241*, 962–971.

Lay, T., J. Hernlund, and B. A. Buffett (2008), Core–mantle boundary heat flow, *Nature Geoscience*, *1*(1), 25–32.

Lekić, V., S. Cottaar, and A. Dziewonski (2012), Cluster analysis of global lower mantle tomography: A new class of structure and implications for chemical heterogeneity, *Earth and Planetary Science Letters*, *357*, 68–77.

Li, M., and A. K. McNamara (2013), The difficulty for subducted oceanic crust to accumulate at the earth's core-mantle boundary, *Journal of Geophysical Research: Solid Earth*, *118*(4), 1807–1816.

Lifshitz, I., and V. V. Slyozov (1961), The kinetics of precipitation from supersaturated solid solutions, *J. Phys. Chem. Solids*, *19*, 35–50, doi:10.1016/0022-3697(61)90054-3.

Lin, S.-C., and P. E. van Keken (2006), Dynamics of thermochemical plumes: 1. Plume formation and entrainment of a dense layer, *Geochemistry, Geophysics, Geosystems*, *7*(2).

Manga, M. (1996), Mixing of heterogeneities in the mantle: effect of viscosity differences, *Geophysical Research Letters*, *23*(4), 403–406.

Martinez, F., and R. Hey (2017), Propagating buoyant mantle upwelling on the Reykjanes Ridge, *Earth and Planetary Science Letters*, *457*, 10–22, doi:http://dx.doi.org/10.1016/j.epsl.2016.09.057.

Masters, G., G. Laske, H. Bolton, and A. Dziewonski (2000), The relative behavior of shear velocity, bulk sound speed, and compressional velocity in the mantle: Implications for chemical and thermal structure, in *Earth's Deep Interior: Mineral Physics and Tomography From the Atlantic to the Global Scale, Geophys. Monogr. Ser.*, vol. 117, edited by S. Karato, A. Forte, R. Liebermann, G. Masters, and L. Stixrude, pp. 63–87, American Geophysical Union, Washington, D. C.

McCarthy, C., and Y. Takei (2011), Anelasticity and viscosity of partially molten rock analogue: Toward seismic detection of small quantities of melt, *Geophysical Research Letters*, *38*(18).

McCarthy, C., Y. Takei, and T. Hiraga (2011), Experimental study of attenuation and dispersion over a broad frequency range: 2. The universal scaling of polycrystalline materials, *J. Geophys. Res.*, *116*, B09207, doi:10.1029/2011JB008384.

McCarthy, C., Y. Takei, and T. Hiraga (2011), Experimental study of attenuation and dispersion over a broad frequency range: 2. The universal scaling of polycrystalline materials, *Journal of Geophysical Research: Solid Earth (1978–2012)*, *116*(B9).

McKenzie, D., J. Jackson, and K. Priestley (2005), Thermal structure of oceanic and continental lithosphere, *Earth and Planetary Science Letters*, *233*(3), 337–349.

McMillan, K. M., R. S. Lakes, R. F. Cooper, and T. Lee (2003), The viscoelastic behavior of β-In3Sn and the nature of the high-temperature background, *Journal of materials science*, *38*, 2747–2754.

McNamara, A. K., and S. Zhong (2005), Thermochemical structures beneath africa and the pacific ocean, *Nature*, *437*(7062), 1136–1139.

McNamara, A. K., E. J. Garnero, and S. Rost (2010), Tracking deep mantle reservoirs with ultra-low velocity zones, *Earth and Planetary Science Letters*, *299*, 1–9.

Mei, S., and D. L. Kohlstedt (2000), Influence of water on plastic deformation of olivine aggregates 1. Diffusion creep regime, *Journal of Geophysical Research*, *105*(B9), 21,457.

Minster, J. B., and D. L. Anderson (1981), A Model of Dislocation-Controlled Rheology for the Mantle, *Philosophical Transactions of the Royal Society of London A: Mathematical, Physical and Engineering Sciences*, *299*(1449), 319–356.

Mitrovica, J. X., and A. M. Forte (2004), A new inference of mantle viscosity based upon joint inversion of convection and glacial isostatic adjustment data, *Earth Planet. Sci. Lett.*, *225*, 177–189, doi:10.1016/j.epsl.2004.06.005.

Montési, L. G., and G. Hirth (2003), Grain size evolution and the rheology of ductile shear zones: from laboratory experiments to postseismic creep, *Earth and Planetary Science Letters*, *211*(1), 97–110.

Moulik, P. (2016), Earth's elastic and density structure from diverse seismological observations, Ph.D. thesis, Columbia University, New York, NY.

Moulik, P., and G. Ekström (2014), An anisotropic shear velocity model of the Earth's mantle using normal modes, body waves, surface waves and long-period waveforms, *Geophysical Journal International*, *199*(3), 1713–1738.

Moulik, P., and G. Ekström (2016), The relationships between large-scale variations in shear velocity, density, and compressional velocity in the Earth's mantle, *Journal of Geophysical Research: Solid Earth*, *121*(4), 2737–2771, doi:10.1002/2015JB012679.

Nakagawa, T., P. J. Tackley, and F. Deschamps (2009), Incorporating self-consistently calculated mineral physics into thermochemical mantle convection simulations in a 3-D spherical shell and its influence on seismic anomalies in Earth's mantle, *Geochemistry, Geophysics, Geosystems*, *10*(3), 1–17, doi:10.1029/2008GC002280.

Nakagawa, T., P. J. Tackley, F. Deschamps, and J. A. Connolly (2010), The influence of MORB and harzburgite composition on thermo-chemical mantle convection in a 3-D spherical shell with self-consistently calculated mineral physics, *Earth and Planetary Science Letters*, *296*(3), 403–412.

Okal, E. A., and B.-G. Jo (1990), Q measurements for PhaseX overtones, *Pure and Applied Geophysics*, *132*(1), 331–362.

Olugboji, T. M., S. Karato, and J. Park (2013), Structures of the oceanic lithosphere-asthenosphere boundary: Mineral-physics modeling and seismological signatures, *Geochemistry, Geophysics, Geosystems*, *14*(4), 880–901.

Podolefsky, N. S., S. Zhong, and A. K. McNamara (2004), The anisotropic and rheological structure of the oceanic upper mantle from a simple model of plate shear, *Geophysical Journal International*, *158*(1), 287–296.

Poirier, J., and R. Liebermann (1984), On the activation volume for creep and its variation with depth in the earth's lower mantle, *Physics of the Earth and Planetary Interiors*, *35*(4), 283 – 293, doi:http://dx.doi.org/10.1016/0031-9201(84)90022-0.

Poirier, J. P., J. Peyronneau, M. Madon, F. Guyot, and A. Revcolevschi (1986), Eutectoid phase transformation of olivine and spinel into perovskite and rock salt structures, *Nature*, *321*, 603–605, doi:10.1038/321603a0.

Priestley, K., and D. McKenzie (2013), The relationship between shear wave velocity, temperature, attenuation and viscosity in the shallow part of the mantle, *Earth Planet. Sci. Lett.*, *381*, 78–91, doi:10.1016/j.epsl.2013.08.022.

Putirka, K. (2008), Excess temperatures at ocean islands: Implications for mantle layering and convection, *Geology*, *36*(4), 283–286.

Quinteros, J., S. Sobolev, and A. Popov (2010), Viscosity in transition zone and lower mantle: Implications for slab penetration, *Geophysical Research Letters*, *37*(9).

Resovsky, J., J. Trampert, and R. D. Van Der Hilst (2005), Error bars for the global seismic Q profile, *Earth and Planetary Science Letters*, *230*(3-4), 413–423.

Ritsema, J., H. van Heijst, and J. Woodhouse (1999), Complex shear wave velocity structure imaged beneath Africa and Iceland, *Science*, *286*, 1925–1928.

Romanowicz, B., and B. Mitchell (2015), 1.25 - Deep Earth Structure: Q of the Earth from Crust to Core, in *Treatise on Geophysics (Second Edition)*, edited by G. Schubert, second edition ed., pp. 789–827, Elsevier, Oxford, doi:http://dx.doi.org/10.1016/B978-0-444-53802-4.00021-X.

Rozel, A. (2012), Impact of grain size on the convection of terrestrial planets, *Geochemistry, Geophysics, Geosystems*, *13*(10).

Rozel, A., Y. Ricard, and D. Bercovici (2011), A thermodynamically self-consistent damage equation for grain size evolution during dynamic recrystallization, *Geophysical Journal International*, *184*(2), 719–728.

Rudolph, M. L., V. Lekić, and C. Lithgow-Bertelloni (2015), Viscosity jump in Earth's mid-mantle, *Science*, *350*(6266), 1349–1352.

Sammis, C. G., J. C. Smith, G. Schubert, and D. A. Yuen (1977), Viscosity-depth profile of the Earth's mantle: Effects of polymorphic phase transitions, *Journal of Geophysical Research*, *82*, 3747–3761, doi:10.1029/JB082i026p03747.

Schilling, J.-G. (1991), Fluxes and excess temperatures of mantle plumes inferred from their interaction with migrating mid-ocean ridges, *Nature*, *352*, 397–403.

Schuberth, B. S. A., H. P. Bunge, and J. Ritsema (2009), Tomographic filtering of high-resolution mantle circulation models: Can seismic heterogeneity be explained by temperature alone?, *Geochemistry, Geophysics, Geosystems*, *10*(5).

Sipkin, S. A., and T. H. Jordan (1979), Frequency dependence of QScS, *Bulletin of the Seismological Society of America*, *69*(4), 1055–1079.

Solomatov, V. (2001), Grain size-dependent viscosity convection and the thermal evolution of the earth, *Earth and Planetary Science Letters*, *191*(3), 203–212.

Solomatov, V., R. El-Khozondar, and V. Tikare (2002), Grain size in the lower mantle: constraints from numerical modeling of grain growth in two-phase systems, *Phys. Earth Planet. Int.*, *129*(3-4), 265–282, doi:10.1016/S0031-9201(01)00295-3.

Solomatov, V. S. (1996), Can hotter mantle have a larger viscosity?, *Geophys. Res. Lett*, *23*, 937–940, doi:10.1029/96GL00724.

Solomatov, V. S., and C. C. Reese (2008), Grain size variations in the Earth's mantle and the evolution of primordial chemical heterogeneities, *Journal of Geophysical Research (Solid Earth)*, *113*, B07408, doi:10.1029/2007JB005319.

Steinberger, B., and A. R. Calderwood (2006), Models of large-scale viscous flow in the Earth's mantle with constraints from mineral physics and surface observations, *Geohyps. J. Int.*, *167*, 1461–1481, doi:10.1111/j.1365-246X.2006.03131.x.

Steinberger, B., and T. H. Torsvik (2008), Absolute plate motions and true polar wander in the absence of hotspot tracks., *Nature*, *452*(7187), 620–623, doi:10.1038/nature06824.

Stixrude, L., and C. Lithgow-Bertelloni (2005), Thermodynamics of mantle minerals - I. Physical properties, *Geophysical Journal International*, *162*(2), 610–632, doi:10.1111/j.1365-246X.2005.02642.x.

Stixrude, L., and C. Lithgow-Bertelloni (2011), Thermodynamics of mantle minerals - II. Phase equilibria, *Geophysical Journal International*, *184*(3), 1180–1213, doi:10.1111/j.1365-246X.2010.04890.x.

Sundberg, M., and R. F. Cooper (2010), A composite viscoelastic model for incorporating grain boundary sliding and transient diffusion creep; correlating creep and attenuation responses for materials with a fine grain size, *Philosophical Magazine*, *90*(20), 2817–2840.

Takei, Y., and B. K. Holtzman (2009), Viscous constitutive relations of solid-liquid composites in terms of grain boundary contiguity: 2. Compositional model for small melt fractions, *Journal of Geophysical Research*, *114*(B6), B06,206.

Takei, Y., F. Karasawa, and H. Yamauchi (2014), Temperature, grain size, and chemical controls on polycrystal anelasticity over a broad frequency range extending into the seismic range, *J. Geophys. Res.*, *119*, 5414–5443, doi:10.1002/2014JB011146.

1421 Takei, Y., F. Karasawa, and H. Yamauchi (2014), Temperature, grain size, and chemical con-
1422 trols on polycrystal anelasticity over a broad frequency range extending into the seismic
1423 range, *Journal of Geophysical Research*, *119*, 5414–5443.

1424 Thielmann, M., A. Rozel, B. Kaus, and Y. Ricard (2015), Intermediate-depth earthquake
1425 generation and shear zone formation caused by grain size reduction and shear heating,
1426 *Geology*, *43*(9), 791–794.

1427 Tsai, V. C., and D. J. Stevenson (2007), Theoretical constraints on true polar wander, *Journal*
1428 *of Geophysical Research*, *112*(B5), B05,415, doi:10.1029/2005JB003923.

1429 Turner, A. J., R. F. Katz, and M. D. Behn (2015), Grain-size dynamics beneath mid-ocean
1430 ridges: Implications for permeability and melt extraction, *Geochemistry, Geophysics,*
1431 *Geosystems*, *16*(3), 925–946.

1432 Vauchez, A., A. Tommasi, and D. Mainprice (2012), Faults (shear zones) in the Earth's man-
1433 tle, *Tectonophysics*, *558–559*(0), 1–7, doi:http://dx.doi.org/10.1016/j.tecto.2012.06.006.

1434 Wagner, C. (1961), Theorie der Alterung von Niederschlägen durch Umlösen (Ostwald-
1435 Reifung), *Zeitschrift für Elektrochemie, Berichte der Bunsengesellschaft für physikalische*
1436 *Chemie*, *65*(7–8), 581–591, doi:10.1002/bbpc.19610650704.

1437 Webb, S., I. Jackson, and J. F. Gerald (1999), Viscoelasticity of the titanate perovskites
1438 CaTiO 3 and SrTiO 3 at high temperature, *Physics Of The Earth And Planetary Interiors*,
1439 *115*, 259–291.

1440 Weis, D., M. O. Garcia, J. M. Rhodes, M. Jellinek, and J. S. Scoates (2011), Role of the deep
1441 mantle in generating the compositional asymmetry of the hawaiian mantle plume, *Nature*
1442 *Geoscience*, *4*(12), 831–838.

1443 Widmer, R., G. Masters, and F. Gilbert (1991), Spherically symmetric attenuation within the
1444 Earth from normal mode data, *Geophysical Journal International*, *104*(3), 541–553.

1445 Workman, R., and S. Hart (2005), Major and trace element composition of the depleted
1446 MORB mantle (DMM), *Earth and Planetary Science Letters*, *231*, 53–72, doi:doi:
1447 10.1016/j.epsl.2004.12.005.

1448 Xu, W., C. Lithgow-Bertelloni, L. Stixrude, and J. Ritsema (2008), The effect of bulk com-
1449 position and temperature on mantle seismic structure, *Earth and Planetary Science Let-*
1450 *ters*, *275*(1-2), 70–79, doi:10.1016/j.epsl.2008.08.012.

1451 Xu, Y., M. E. Zimmerman, and D. L. Kohlstedt (2004), Deformation behavior of partially
1452 molten mantle rocks, in *Rheology and Deformation of the Lithosphere at Continental Mar-*
1453 *gins*, vol. 1, edited by G. D. Karmer, B. Taylor, N. W. Driscoll, and D. L. Kohlstedt, pp.

284–310, Columbia University Press.

Yamauchi, H., and Y. Takei (2016), Polycrystal anelasticity at near-solidus temperatures, *Journal of Geophysical Research-Solid Earth*, *121*(11), 7790–7820.

Yamazaki, D., T. Yoshino, and T. Nakakuki (2014), Interconnection of ferro-periclase controls subducted slab morphology at the top of the lower mantle, *Earth Planet. Sci. Lett.*, *403*, 352–357, doi:10.1016/j.epsl.2014.07.017.

Yang, T., and M. Gurnis (2016), Dynamic topography, gravity and the role of lateral viscosity variations from inversion of global mantle flow, *Geophysical Journal International*, *207*(2), 1186, doi:10.1093/gji/ggw335.

Zhao, S., Z. Jin, J. Zhang, H. Xu, G. Xia, and H. W. Green, II (2012), Does subducting lithosphere weaken as it enters the lower mantle?, *Geophys. Res. Lett*, *39*, L10311, doi:10.1029/2012GL051666.